Title
THE JET-DISK SYMBIOSIS .2. INTERPRETING THE RADIO/UV CORRELATIONS IN QUASARS

Journal
ASTRONOMY & ASTROPHYSICS, 298(2)

ISSN
0004-6361

Authors
FALCKE, H
MALKAN, MA
BIERMANN, PL

Publication Date
1995

Peer reviewed

The jet-disk symbiosis
II. Interpreting the Radio/UV correlations in quasars

Heino Falcke[1], Matthew A. Malkan[2], Peter L. Biermann[1]

Max-Planck Institut für Radioastronomie, Auf dem Hügel 69, D-53121 Bonn, Germany[1]
Department of Astronomy, UCLA, Los Angeles, CA 90024-1562, USA[2]

Astronomy & Astrophysics, in press [astro-ph/9411100]

Abstract

We investigate the correlation between the accretion disk (UV) luminosity and the radio core emission of a quasar sample, containing all PG quasars, also deriving empirical conversion factors from emission line luminosities to disk luminosities. This method allows us to investigate the radio properties of AGN on the absolute scale set by the accretion power. In a radio vs. $L_{\rm disk}$ plot we find the quasars to be separated into four classes: core dominated quasars (CDQ), lobe dominated quasars (LDQ), radio-intermediate quasars (RIQ) and radio weak quasars. In general the radio core emission scales with the disk luminosity, especially in the radio weak quasars. This shows that radio and UV emission have a common energy source and that the difference between radio loud and radio weak is established already on the parsec scale. We investigate the possibility that radio jets are responsible for the radio core emission in radio loud and radio weak quasars. Comparing our data with a simple jet emission model that takes the limits imposed by energy and mass conservation in a coupled jet-disk system into account, we find that radio loud jets carry a total power $Q_{\rm jet}$ that is at least 1/3 of the observed disk luminosity $L_{\rm disk}$. The strong radio core emission in radio loud quasars relative to $L_{\rm disk}$ is difficult to explain by normal acceleration of thermal electrons into a non-thermal powerlaw distribution. One rather is forced to postulate an efficient process producing a large number of pairs and/or injecting electrons with a distribution with low-energy cut-off around 50 MeV – secondary pair production in hadronic cascades could be such a process. Width and shape of the UV-radio correlation of LDQ and CDQ limit the parameter range for the bulk Lorentz factor of the jet to a narrow region ($3 \leq \gamma_{\rm j} \leq 10$)). The radio emission of radio weak quasars can be explained with exactly the same parameters for a powerful relativistic jet if secondary pair production, as suggested for radio loud jets, is inhibited. There is evidence that RIQ are the relativistically boosted population of radio weak quasar jets. Our diagram provides also a test for the unification of FR II radio galaxies with quasars as we can estimate the hidden disk luminosity of FR II galaxies and find that this is consistent with FRII being misdirected quasars.

Keywords: galaxies: active – galaxies: jets – galaxies: nuclei – accretion disks

1 Introduction

The standard picture for the active galactic nuclei (AGN) of galaxies classified as quasars still is an accreting supermassive black hole surrounded by an accretion disk. The release of energy due to the infall in the gravitational potential is thought to be responsible for the enormous energy output seen in the optical to ultraviolet (UV) which is able to dominate the total emission of the underlying galaxy. While for individual sources the spectral energy distribution (SED) may be dominated by other contributions, e.g. gamma-rays, the UV emission in general is assumed to be the major channel for the energy release of quasars. High gamma-ray fluxes occur only in a few sources and are obviously boosted. However, recently it was pointed out that relativistic jets in radio loud quasars may be another important channel for expelling high amounts of energy from the central engine (Rawlings & Saunders 1991, hereafter RS91; Falcke, Mannheim, Biermann 1993b, hereafter FMB; Falcke & Biermann 1994b, hereafter *Paper I*; Celotti & Fabian 1993). Although the radiative contribution of jets to the SED in the radio and gamma regime is small, their energy flow in bulk relativistic motion, magnetic energy and relativistic particles may be a substantial fraction of total energy released from the central engine. Such a powerful jet suggests that this kind of outflow is directly coupled to the accretion process in the very vicinity of the black hole – where most of the energy is released – and will have a strong impact on the disk itself. Therefore one can not treat disk and jet as two isolated parts but must treat them as a coupled sytem.

Send offprints requests to: HFALCKE@mpifr-bonn.mpg.de

In previous papers (*Paper I*, FMB) we studied the standard theory for the radio emission of compact radio cores produced by radio jets in quasars considering especially the link between the jet and an accretion disk as the basic source for energy and matter. This is simply the Blandford & Königl (1979) theory plus energy and mass conservation in the jet-disk system.

A necessary consequence of this jet-disk link is the scaling of the emission from the compact radio core in galactic nuclei with the disk luminosity radiated in the UV where the scaling is not necessarily linear. Another conclusion was that for a given accretion rate, the core emission of radio loud jets is already close to the maximum efficiency, and brighter emission is only possible by relativistic boosting. Moreover Falcke & Biermann (1994b) introduced the concept of a jet-disk symbiosis and started with the basic Ansatz that jets are necessary partners of accretion disks around compact objects, and not fortuitous by-products of disks. In this context the question was raised whether the radio emission of radio-weak quasars could be explained by the same kind of relativistic jets as well but being less efficient in accelerating electrons. The predictions are that UV and radio core emission should be strongly correlated in radio weak quasars as well and that boosted radio weak jets with enhanced variable radio emission are found. Obviously depends the dichotomy of the radio emission on the host galaxy (radio loud: elliptical, radio weak: spiral) and it is hard to understand why the basic parameters of jet flows should differ as a function of the host galaxy when the production happens very close to the black hole where the effects of the host galaxy should be negligible.

In this paper we now want to test some of these ideas and see if they contradict available observational data. If there is indeed a fundamental process linking accretion process and jet production, it should be insensitive to the environment and the host galaxy except for the bimodality between radio loud and radio weak quasars. Further out the environmental impact of the host galaxy will inevitably change the appearance of the jet and disk and modify the emission region. Therefore one has to select carefully the observational data for each object, and must make sure that the observed radiation reflects the physical situation of the center and not of the outer region. To achieve this we can follow two extreme strategies, one is to have very high spatial resolution of the observation e.g. by looking at nearby galactic nuclei. The other extreme would be to look at very luminous objects, where the central engine outshines all other sources in a galaxy like in quasars. Here we will follow the second approach and leave the nearby nuclei – with the exception of our Galactic Center, which is discussed in Falcke et al. (1993a&b), Falcke & Biermann (1994a&c) and Falcke (1994a&b), to future work. All other galactic nuclei, e.g. Seyfert and radio galaxies, are very difficult to use as test candidates as it requires an elaborated scheme to separate the contributions from different parts of the galaxy (e.g. starburst and AGN).

We build on the work by Miller et al. (1993a, MSR) who investigated the optically selected PG bright quasar sample and found correlations between radio and optical line emission luminosities of radio weak quasars. We now extend this analysis by enlarging the sample with more sources and comparing it with FR II galxies in light of current unification theories. Moreover we try to determine the disk luminosities of the quasars in our sample as accurately as possible from existing data to compare disk and radio power in absolute terms. This allows us to constrain strongly the parameter range of radio jets and also give a solid classification for the radio properties of quasars.

In Sec. 2 of this paper we introduce our sample and present our method to estimate the disk luminosity of the individual quasars and calibrate different other indicators to obtain empirical conversion factors, e.g. from line luminosities to disk luminosities. Section 3 describes the available radio data and Sec. 4 the UV-radio diagram and its implication for the different classes of quasars. In Sec. 5 we discuss the constraints this diagram imposes on jet parameters like Lorentz factor and total jet power. Section 5 discusses the implication of our estimated parameters for the unification of quasars and FR II radio galaxies and provides a simple method to estimate the hidden disk luminosity in radio galaxies.

For consistency with some of the observational papers we use $q_0 = .5$ and $H_0 = 50$ km/sec/Mpc as cosmological parameters.

2 The disk luminosity

2.1 The quasar sample

Most quasars show a fairly homogenous SED with two important features – an infrared (IR) and an UV-bump (Edelson and Malkan 1986; Sanders et al. 1989). While the IR seems to be due to thermal emission from dust, the dominant UV bump probably reflects the spectrum of an accretion disk around a supermassive black hole (Malkan & Sargent 1982, Malkan 1983). We now estimate this UV-bump luminosity – which hereafter we will also refer to as 'disk luminosity' ($L_{\rm disk}$) – as accurately as possible.

We take the observationally best studied sample of quasars namely the PG sample of bright quasars (Schmidt & Green 1983) with redshift $z < 0.5$ with a multitude of published observational data. Boroson & Green (1992, hereafter BG92) presented a thorough study of the emission line properties of this sample while Sun & Malkan (1989, hereafter SM89) determined the disk luminosity from fitting disk spectra to optical and UV data for a sample containg many of the PG quasars. Kellermann et al. (1989, hereafter KSSSG) and Miller et al. (1993, hereafter MSR) published radio data obtained with the VLA. MSR also tried to classify the morphological structure of the radio maps and studied correlation between radio fluxes and emission lines.

The low redshift PG sample ($z < 0.5$) we will mainly base our arguments on is given in Table 1 and contains 87 sources (#1-#87). We did not include the recent addition PG 1001+054 (not included in BG92) or PG 0119+229, since it shows no broad lines. In addition we will consider an extended sample which cannot be used for statistical purposes, as it is not complete and has no clear defined selection criterion. Sources #88-#113 in Tab. 1 are the PG quasars with $z > 0.5$ which were measured by KSSSG as well but not discussed by MRS. It is known that there are some selection effects for the PG sample with $z > 0.5$ (Wampler & Ponz 1985). Beyond the whole PG sample we have the sources #113-#131 which (with the exception of 1821+643) were included in the sample of SM89 and had disk fits available.

Besides quasars we will discuss briefly a sample of Fanaroff-Riley type II (FRII) radio galaxies with $z < 0.5$ which are selected from the 3C-based sample of Laing et al. (1983) and were investigated further by Rawlings et al. (1989) and RS91. It contains 39 FR II galaxies and is listed in Table 2 (#132-#170). The Laing et al. (1983) sample is 96% complete to a flux density limit of 10 Jy at 178 Mhz for sources smaller than 10'and can be considered as fairly unbiased because unboosted lobe emission dominates the whole spectrum at this low frequency.

2.2 The UV-bump

SM89 fitted accretion disk spectra to a variety of quasars. They collected IR to UV data from a sample of quasars – most of them belonging to the PG sample – and used standard relativistic thin accretion disk models including the effects of rotating black holes for their fits of the 'UV-bump'. They also assumed an underlying powerlaw, which is no longer state of the art, but does not invalidate neither their nor our conclusions although it might introduce a slight and systematic shift in the luminosities.

From this detailed study we will mainly use one important number, namely the *fitted* luminosity of the UV-bump. This number may differ from the total integrated luminosity of the measured UV-bump, as the fitted spectra do not always interpolate the observed data perfectly well, indicating the presence of other components not explained by and not necessarily linked to a standard accretion disk. In column 6 ('UV') of Table 1 we listed this number from SM89 for all objects, where we assumed an average inclination angle of 40° for the disks.

Unfortunately, SM89 did not include all PG quasars in their investigation, we therefore looked into the archived data of this study and found a few more PG quasars with yet unpublished data. Using exactly the same method as SM89, we were able to obtain some more disk fits for these objects and included them in our list. The new sources are indicated with an asterisk in Table 1: PG 0007+106, 0232−042, 0906+484, PG 1352+011, PG 1411+442, PG 1501+106, PG 1522+101, PG 1613+658, PG 1634+706, 2041−105, and PG 2302+029. We will refer to the whole sample of sources having UV-bump fits available (published or unpublished) simply as the SM89 sample.

In the following we assume that the luminosities derived from the UV-bump fits are indeed the 'disk luminosity'. Because the PG sample is so well studied we now have a large number of quasars having disk fits and several other luminosity indicators available, such as emission line luminosities and monochromatic continuum luminosities. As it is generally accepted that these emission lines are produced through ionization by the central source we can now compare UV-bump fits and emission lines to get empirical conversion factors. For sources where no fits are available we then can use monochromatic luminosities and emission line luminosities to get estimates for the disk luminosity from these numbers alone. For an individual source there may be discrepancies between the 'real' value and the estimated disk luminosity but in a statistical sense we will get reliable numbers.

Of course this works only if the correlations are almost linear and depend on one parameter only, i.e. the disk luminosity. That this is indeed the case is not obvious a priori. For example, an emission line responds not only to an increase in the luminosity, but also to a frequency shift of the exciting spectrum which in accretion theory happens due to a shift in mass and accretion rate of the black hole. Fortunately, the dependence of the shift in frequency ($T_{\rm eff}$) is weak – $T_{\rm eff} \propto \dot{M}_{disk}^{.25}/M_\bullet^{.5}$ while $L_{\rm disk} \propto \dot{M}_{\rm disk}$. If all quasars radiate close to the Eddington luminosity, then we have $T_{\rm eff} \propto M_\bullet^{-.25}$. In this sense the PG quasars are relatively uniform – they have comparable effective temperatures of several 10^4 Kelvin – and the expected relations should be fairly independent of the black hole mass, but one has to remember that they will become inadequate if $T_{\rm eff}$ changes

appreciably. Some Seyfert galaxies for example show a bump which peaks somewhere in the soft x-ray regime and they should deviate systematically from such correlations. There may also be plenty other (e.g. environmental) effects influencing the emission line strength and one should be extremely carefull in extrapolating the relations presented in the next section to other luminosity regimes or even other quasar samples. The reason we can use the simple conversion here is the uniformity of the PG quasars which were all selected as objects with a blue excess – but even there the conversion from line luminosity to $L_{\rm disk}$ will be only correct in a statistical sense and may be completely wrong for some individual sources (see for example PG 1008+133 and PG 1206+459).

2.3 Monochromatic continuum luminosities

A very good indicator for the disk luminosity are the absolute blue magnitude $M_{\rm b}$ – which is not surprising as it was used to select the quasars in this sample – and the absolute magnitude $M_{\rm v}$ of the continuum at λ5500 of the core spectrum in the restframe of the quasar (BG92). We corrected the magnitudes given in BG92 for the different value $q_0 = 0.5$ we use in our paper. The flux F_ν at $\nu = 5.45 \cdot 10^{14}$ Hz ($\lambda = 5500$Å) can be converted to $M_{\rm v}$ by the formula

$$\begin{aligned} M_{\rm v} &= -2.5 \lg \left(\frac{F_\nu}{3.53 \cdot 10^{-20} {\rm erg/sec/Hz}} \right) \\ &\quad +5 \lg \left(\frac{D_{l_\nu}}{\rm pc} \right) - 5 \end{aligned} \tag{1}$$

and the monochromatic luminosity distance for our set of cosmological parameters as a function of redshift is

$$D_{l_\nu} = 1.2 \cdot 10^{10} \,{\rm pc} \, \left(\sqrt{1+z} - 1 \right). \tag{2}$$

In Fig. 1a+b we plotted the relation between these colors and the disk luminosity from SM89. In all cases the slope of the correlation between color and luminosity found with linear regression is within the errors 0.4 – compatible with a direct proportionality between the luminosity in the blue color and the total luminosity. We therefore fixed the slope at that value and determined the intersection to a high precision.

$$\lg L_{\rm disk}\,(M_{\rm b}) = (-0.4 M_{\rm b} + 35.90 \pm 0.04) \pm 0.29 \tag{3}$$

$$\lg L_{\rm disk}\,(M_{\rm v}) = (-0.4 M_{\rm v} + 35.70 \pm 0.04) \pm 0.24. \tag{4}$$

The first error gives the uncertainty in the determination of the offset and the second error the standard deviation of the sample. As one can see in Fig. 1 the correlation indeed is very tight and at least for our sample we can expect that the disk luminosities inferred from $M_{\rm b}$ with help of Eq.(3) will be close to the fitted one. Two sources (PG 1008+133 & PG 1206+459) showed extremely high deviations (more than a factor 10 above the median deviation) in the $L_{\rm disk} - M_{\rm b}$ correlation and we excluded them from this fit. Their extreme deviation seems to indicate an intrinsic and qualitative difference from the other sources and is probably not of statistical origin. Further investigation of these two sources is clearly indicated.

2.4 Emission lines

Another often used indicator for the disk luminosity is the luminosity of the emission lines seen in the optical spectrum. BG92 published a list of spectral data of all low redshift PG quasars and once again we use the SM89 quasars as calibrators for the disk luminosity. In Fig. 1c-e we show the relations between the luminosity in the emission lines (He II, Hβ and O III) and the luminosity of the disk. We make use of the definition in BG92 where for an emission line EL with equivalence width EW the absolute magnitude of this line is given by $M_{\rm [EL]} = M_{\rm v} - 2.5 \lg({\rm EW[EL]})$.

$$\lg L_{\rm disk}\,(M_{\rm HeII}) = (-0.4 M_{\rm HeII} + 34.93 \pm 0.08) \pm 0.41 \tag{5}$$

$$\lg L_{\rm disk}\,(M_{\rm H\beta}) = (-0.4 M_{\rm H\beta} + 33.70 \pm 0.04) \pm 0.22 \tag{6}$$

$$\lg L_{\rm disk}\,(M_{\rm OIII}) = (-0.4 M_{\rm OIII} + 34.45 \pm 0.08) \pm 0.44 \tag{7}$$

For our use it may be simpler but equally effective to use a total luminosity of all lines and calculate a total emission line luminosity. By adding all lines together

$$\begin{aligned} M_{\rm lines} = M_{\rm v} - 2.5 \lg \left(EW[{\rm HeII}] \right. &+ EW[{\rm H}\beta] \\ &+ \left. EW[{\rm O\ III}] \right) \end{aligned} \tag{8}$$

(will be inserted later)

Figure 1: Relation between the disk luminosity obtained from accretion disk fits to the UV-bump by SM89 and (a) the blue magnitude, (b) the visual magnitude and (c-e) emission line luminosities (He II, H β, O III and (f) sum of all lines $M_{\rm lines}$) measured by Boroson & Green (1992) for PG quasars (from top left to bottom right).

we get (Fig. 1f)

$$\lg L_{\rm disk}\,(M_{\rm lines}) = (-0.4 M_{\rm lines} + 33.60 \pm 0.04) \pm 0.24. \qquad (9)$$

We found that the exact combination of the different line luminosities (i.e. by using certain weights) did not really influence the result. The good correlations we find show that we are not subject to severe orientation dependent effects as far as the determination of the disk luminosity is concerned although some of the line luminosities usually are considered isotropic and others not. Nevertheless, H_β shows the tightest correlation and due to its large luminosity it dominates $L_{\rm disk}\,(M_{\rm lines})$. Comparing the correlation of the emission lines with the $M_{\rm v}$ correlation one can see that there is neither a tremendous gain nor a big loss in accuracy by using emission line fluxes instead of continuum fluxes. Both methods therefore seem to be equally suitable to estimate the disk luminosity.

2.5 Average disk luminosity

For the comparison between disk luminosity and radio emission, we make use of an average disk luminosity obtained by taking the geometrical mean from all available luminosity indicators (UV-bump, $M_{\rm v}$, $M_{\rm b}$, $M_{\rm lines}$) of each source where the disk fit was weighted by a factor three. The factor three was used to assure that the fitted $L_{\rm disk}({\rm UV-bump})$ is not dominated by the indirectly inferred numbers $L_{\rm disk}(M_{\rm b})$, $L_{\rm disk}(M_{\rm v})$ and $L_{\rm disk}(M_{\rm lines})$ which in our sample come in triplicate. The geometric mean was choosen because the derivation of the conversion factors and the subsequent discussion takes place in the log/log plane – the geometric mean is just the arithmetic mean of the log.

As seen in Table 1 in most quasars all methods to derive the disk luminosity yield similar results with a scattering smaller than a few tenth in the log. This confirms our optimism in anticipating that the luminosity indicators are fairly reliable in a statistical sense. Only a few exceptional cases show deviations larger than a factor three. These quasars, indicated with daggers in Table 1, have shown large continuum variations between their photographic measurement in the PG survey and the later spectrophotometry used for disk model fitting.

3 The radio data

From observations we know that the radio spectrum of the compact cores in radio loud quasars is flat and fairly independent of the frequency. This is readily explained as the overlap of several synchrotron spectra in a gradually declining magnetic field along the jet cone (Blandford & Königl 1979). Generally the observation of a core at one frequency is equivalent with probing the jet at a certain distance from the origin but as long as the spectrum is basically flat, one frequency tells as much as any other. In contrast to a black body spectrum the shift of the flat non-thermal spectrum in frequency would hardly make any difference in the observed flux. Hence we do not need to integrate the whole spectrum to get a radio luminosity in analogy to the UV luminosity. For our comparison the monochromatic luminosity at one radio frequency alone is adequate. In *Paper I* we speculated that the compact radio emission in radio weak quasars might be due to jets as well following the same basic principles as their radio loud counterparts. Consequently this and the following considerations may apply to radio weak quasars as well. Unfortunately only a few radio weak cores have been measured reliably at high radio frequencies. Antonucci & Barvainis (1988) for example find a high frequency excess in 9 out of 17 objects at $\lambda 2$ cm which could be attributed to a flat spectrum core.

The radio data we took are primarily from Miller et al. (1993) for the low redshift PG sample and from Kellermann et al. (1989) for the rest of the sample; they give a list of VLA fluxes at 5 GHz. 79 out of 89 quasars were detected and in 50 cases a central compact core was also clearly seen. We added, if available, photometric radio data from the NASA Extragalactic Database (NED), from a catalog of Markarian galxies available at the MPIfR (Sherwood, W. p.c.) and other available literature (see Notes). We then transformed the spectra into the rest frame of the quasars and fitted powerlaws or 3rd order polynomials for each source. In cases where multiple photometric datapoints were available at one frequency and the source was variable, we took the geometric mean of the data. For sources without spectral informations we assumed an spectral

Figure 2: Monochromatic luminosity of the compact radio core vs. the disk luminosity (see text) for PG quasars with $z < 0.5$. 'D': PG quasars showing lobes, 'P': radio loud PG quasars appearing as point sources, *boxes*: RIQ, *black dots*: radio weak point sources, *dots with shades*: radio weak sources with extended emission, *grey dots with cross*: radio weak PG quasars with $z > .5$, *grey dots without cross*: radio weak quasars from SM89, *grey open circles with cross:* radio loud PG quasars with $z > 0.5$, *grey open circles without cross:* radio loud quasars from SM89, *circles and boxes with grey background:* flat spectrum sources.

index of $\alpha = -0.5$. Thus we obtained fairly accurate total fluxes at 5 GHz in the rest frame of the quasar. For the core fluxes we did the same, however, as we have data only at one frequency we simply assumed a flat spectrum ($\alpha = 0$) to get the 5 GHz rest frame flux. In the cases where the extended emission swamps the core or the quasars were not detected at all, we took the limits for the core fluxes or the limits of the total fluxes respectively. For a few sources among those not belonging to the PG sample where no core fluxes were available, we either estimated an upper limit for a flat spectrum core flux from the steep spectrum at high frequencies or assumed a median value of the core/lobe ratio of 0.72 found from our (radio weak) sample for Mkn 132, Mkn 679 and 1821+643 and of 0.15 (from double lobed sources) for 3C 110 and 3C 232. We classified the radio spectra, which are shown in Falcke (1994a), according to their slope at 5 GHz in the rest frame as flat (F) or steep (S) and also marked obviously variable (V) spectra. These classifications and the monochromatic core luminosities are presented in Table 1 as well.

4 The UV-radio correlation

In Fig. 2 we plotted the 5 GHz radio core flux versus the average disk luminosity determined from all available luminosity indicators for each quasar (Sec. 2.5). In Fig. 2 radio cores of radio weak quasars are represented by black dots and an arrow indicates upper limits for the detection of a compact core. In the few cases where the quasar was not detected at all, we used only the arrow. Radio weak quasars showing extended emission are marked with a grey shade around the black dot.

Cores of radio loud quasars are given by open circles and boxes. Point sources are marked with a 'P', double lobed sources with a 'D' and flat spectrum sources by a grey filling.

To complete the picture, we also added the sources belonging to the extended sample in grey. Those sources belonging to the high redshift PG quasar sample are marked with an additional cross.

The quasars fall in at least three distinct categories: radio weak, radio loud lobe dominated quasars (LDQ) and flat spectrum core dominated quasars (CDQ). The distinction between radio-loud and radio-weak holds not only for the total flux, but also for the core fluxes. The separation needs to be undestood relative to the disk luminosities. There may be radio weak quasars with a high accretion rate which have more luminous radio cores than some low accreting radio loud objects. Considering only the core fluxes, CDQ are the brightest population. This diagram confirms the well accepted idea that flat spectrum CDQ are the consequence of orientation effects in conjunction with relativistic boosting, which leads to a strong enhancement of the core flux relative to the un-boosted lobes and disk luminosities.

A few sources do not fit into this general trend: the flat spectrum variable point sources with no sign of large scale lobe structure and a relatively low accretion rate with $L_{\rm disk} < 10^{46}$ erg/sec (boxes in Fig. 2). They have overall properties of (boosted) CDQ but are relatively less luminous and rather seem to fall on the extrapolation of LDQ. Following MRS, we will call these sources radio-intermediate quasars (RIQ) and discuss them in more detail later.

There is a clear correlation between the disk luminosity and the radio core fluxes in each subgroup. Despite the many uncertainties involved, this correlation is remarkably good for extragalactic astrophysical data but not surprising; radio power an NLR luminosity are also well correlated in these galaxies (see Wilson 1992). It is noteworthy that the upper limits also agree well with the general trend so that a non-detection does not necessarily mean that there is no radio emission, but that the sensitivity was insufficient to measure a radio jet which belongs to a quasar with this redshift and accretion rate. Our theoretical arguments imply that they should be detectable with higher sensitivity (below the 100μJy level). All correlations remain when fluxes, rather than luminosities, are plotted.

We stress that the radio cores of radio loud quasars (i.e. LDQ and CDQ) are brighter than the cores of radio weak quasars at the same disk luminosity. As we know from numerous VLBI observations that the bulk

#	name	z	class	$L_{\rm disk}$	$L_{\rm disk}$ UV	$L_{\rm disk}$ Mb	$L_{\rm disk}$ Mv	$L_{\rm disk}$ lines	Radio at 5 GHz νL_ν	Radio at 5 GHz $f_{\rm c}(\%)$	Radio at 5 GHz α
1	0003+158,PG	0.45	L,S,D	46.3	-	46.3	46.4	46.4	42.5	30.	-0.8
2	0003+199,PG,Mkn335	0.025	Q,P	44.6	44.6	44.7	44.5	44.6	38.6	80.	-0.29
3	0007+106,PG,IIIZw2*	0.089	L,F,V	45.3	45.4	44.8	45.2	45.3	41.6	50.	0.62
4	0026+129,PG	0.142	Q,E	45.6	-	45.7	45.5	45.5	<39.2	<7.	-0.5
5	0043+039,PG	0.384	Q	46.	45.8	46.2	46.1	46.	39.7	90.	-0.5
6	0049+171,PG	0.064	Q,P	44.6	-	44.6	44.4	44.7	38.7	100.	-0.5
7	0050+124,PG,IZW1	0.06	Q,P	45.	44.9	45.2	45.2	45.	39.1	70.	-0.77
8	0052+251,PG	0.155	Q,E	45.5	-	45.6	45.5	45.5	39.3	60.	-0.5
9	0157+001,PG,MK1014	0.164	Q,P	45.6	-	45.7	45.5	45.6	40.4	60.	-1.
10	0804+761,PG	0.1	Q,E	45.4	-	45.3	45.4	45.5	39.3	40.	-0.5
11	0838+770,PG	0.131	Q	45.	-	45.1	45.	45.	<38.7	<90.	-0.5
12	0844+349,PG,TON 951	0.064	Q	44.9	44.7	45.4	45.	44.9	<38.4	<100.	-0.5
13	0921+525,PG	0.035	Q,E	44.3	-	44.2	44.2	44.5	38.7	50.	-0.87
14	0923+129,PG,Mrk705	0.029	Q,P	44.3	-	44.3	44.3	44.3	38.7	30.	-0.5
15	0923+201,PG	0.19	Q	45.5	-	45.5	45.5	45.6	<39.2	<90.	-0.5
16	0934+013,PG	0.05	Q,E	44.3	-	44.2	44.2	44.4	<38.2	<60.	-0.5
17	0947+396,PG	0.206	Q	45.4	-	45.4	45.3	45.4	<39.3	<90.	-0.5
18	0953+414,PG	0.239	Q,E	46.1	46.2	46.1	45.9	46.1	<39.2	<9.	-0.5
19	1001+054,PG	0.161	Q,E	45.3	-	45.3	45.3	45.2	<39.4	<60.	-0.5
20	1004+130,PG,4C13.41	0.24	L,S,D	45.9	46.	45.7	46.	45.6	41.4	5.	-1.
21	1011−040,PG	0.058	Q,P	44.6	-	44.7	44.7	44.5	38.3	100.	-0.5
22	1012+008,PG	0.185	Q,P	45.6	-	45.5	45.5	45.6	39.7	70.	-0.5
23	1022+519,PG	0.045	Q,E	44.2	-	44.2	44.2	44.1	38.	60.	-0.5
24	1048−090,PG	0.344	L,S,D	46.	-	46.	45.9	45.9	42.	7.	-0.88
25	1048+342,PG	0.167	Q	45.5	-	45.5	45.2	45.6	<39.	<90.	-0.5
26	1049−005,PG	0.357	Q,E	46.1	-	46.1	46.	46.1	<39.7	<60.	-0.5
27	1100+772,PG,3C249.1	0.313	L,S,D	45.9	45.9	46.	46.	46.	42.	8.	-0.99
28	1103−006,PG	0.425	L,S,D	46.	46.	46.2	46.	45.9	42.4	20.	-0.55
29	1114+445,PG	0.144	Q	45.1	45.	45.3	45.2	45.3	<38.9	<90.	-0.5
30	1115+407,PG	0.154	Q	45.1	-	45.3	45.1	44.9	<39.	<70.	-0.5
31	1116+215,PG	0.177	Q,P	45.9	-	45.8	45.9	46.1	40.	70.	-0.5
32	1119+120,PG	0.049	Q,E	44.7	-	44.9	44.7	44.5	<38.2	<30.	-0.5
33	1121+422,PG	0.234	Q	45.5	-	45.7	45.4	45.4	<39.2	<90.	-0.5
34	1126−041,PG	0.06	Q	44.8	-	44.7	44.9	44.9	<38.4	<70.	-0.5
35	1149−110,PG	0.049	Q,E	44.5	-	44.6	44.4	44.6	38.8	50.	-0.5
36	1151+117,PG	0.176	Q	45.5	45.5	45.6	45.3	45.3	<39.	<90.	-0.5
37	1202+281,PG,GQ COM	0.165	Q,P	45.4	45.3	45.8	45.1	45.3	39.5	80.	-0.5
38	1211+143,PG	0.085	Q	45.5	45.5	45.4	45.5	45.5	<39.	<60.	-0.5
39	1216+069,PG	0.334	Q,P	46.1	-	46.1	46.1	46.1	40.8	90.	-0.5
40	1226+023,PG,3C273	0.158	L,F,V	46.6	46.7	46.6	46.5	46.5	44.1	70.	-0.085
41	1229+204,PG,TON 1542	0.064	Q	44.9	44.9	45.1	44.9	45.	<38.7	<90.	-0.5
42	1244+026,PG	0.048	Q,E	44.1	44.	44.3	44.4	44.2	38.4	60.	-0.5
43	1259+593,PG	0.472	Q	46.4	46.5	46.5	46.3	46.	<39.8	<80.	-0.5

Table 1: The quasar sample used in this paper. (#1-#87) is the PG sample with $z < 0.5$, (#88-#113) is the rest of the PG sample, and (#114-#131) are quasars from the sample of SM89. Col. (1): ID number, Col (2): IAU name; Col. (3): redshift, Col. (4): radio classification Q – radio weak, L – radio loud, S – steep spectrum ($\alpha \leq -0.5$), F – flat spectrum ($\alpha > -0.5$), V – variable spectrum, P – point source, E - extended emission, D – (double) lobe structure; Col. (5): average disk luminosity; Col. (6-9): disk luminosities derived from (6) UV-bump fits, (7) $M_{\rm b}$, (8)continuum at λ5500 rest frame, (9) emission lines; Col. (10): radio luminosity of the core at 5 GHz rest frame, Col. (11): ratio of core flux to total flux at 5 GHz rest frame in per cent; Col. (12): differential spectral index of fitted spectrum at 5 GHz rest frame. An asterisk (*) marks quasars with new accretion disk fits and a dagger (†) marks the 2 quasars with strong variations between $M_{\rm b}$ and the UV.

#	name	z	class	$L_{\rm disk}$	$L_{\rm disk}$ UV	Mb	Mv	lines	Radio at 5 GHz νL_ν	$f_{\rm c}(\%)$	α
44	1302−102,PG	0.286	L,F,V	46.1	-	46.2	46.3	45.8	43.	100.	0.035
45	1307+085,PG	0.155	Q	45.5	45.5	45.6	45.5	45.6	39.2	90.	-0.5
46	1309+355,PG	0.184	L,F,P	45.5	-	45.7	45.5	45.3	41.4	90.	-0.5
47	1310−108,PG	0.035	Q	44.3	-	44.2	44.2	44.5	<37.8	<100.	-0.5
48	1322+659,PG	0.168	Q	45.4	-	45.5	45.3	45.3	39.	90.	-0.5
49	1341+258,PG	0.087	Q	44.8	-	44.8	44.7	44.8	<38.5	<100.	-0.5
50	1351+236,PG	0.055	Q,E	44.4	-	44.5	44.6	44.1	<38.2	<40.	-0.5
51	1351+640,PG	0.087	L,F,P	45.2	-	45.1	45.3	45.2	40.7	100.	-0.14
52	1352+183,PG	0.158	Q	45.4	-	45.5	45.3	45.4	39.	90.	-0.5
53	1354+213,PG	0.3	Q	45.5	-	46.	45.3	45.2	<39.3	<90.	-0.5
54	1402+261,PG	0.164	Q,P	45.4	-	45.6	45.4	45.3	39.3	70.	-0.5
55	1404+226,PG	0.098	Q,P	44.8	-	45.	44.8	44.5	39.1	70.	-0.5
56	1411+442,PG*	0.089	Q,P	45.3	45.5	45.3	45.1	45.1	38.9	90.	-0.5
57	1415+451,PG	0.114	Q	45.	-	45.2	45.	44.7	<38.8	<70.	-0.5
58	1416−129,PG	0.129	Q,E	45.3	45.1	45.4	45.5	45.8	39.4	20.	-0.5
59	1425+267,PG,TON 202	0.366	L,S,D	45.9	45.8	46.2	46.1	46.1	41.9	20.	-0.75
60	1426+015,PG,Mkn1383	0.086	Q,P	45.3	45.4	45.2	45.3	45.2	39.2	90.	-0.5
61	1427+480,PG	0.221	Q	45.4	-	45.5	45.2	45.5	<39.2	<90.	-0.5
62	1435−067,PG	0.129	Q	45.4	-	45.4	45.3	45.4	<38.8	<90.	-0.5
63	1440+356,PG	0.077	Q,E	45.	-	45.1	45.	44.9	38.8	40.	-1.1
64	1444+406,PG	0.267	Q	45.7	-	45.8	45.7	45.5	<39.2	<90.	-0.5
65	1448+273,PG	0.065	Q,P	44.9	-	45.	45.	44.7	38.9	100.	-0.5
66	1501+106,PG,Mkn841*	0.036	Q,E	44.9	45.1	44.4	44.8	45.	38.3	50.	-0.81
67	1512+370,PG,4C37.43	0.371	L,S,D	46.	46.	46.1	46.	46.2	42.1	20.	-0.71
68	1519+226,PG	0.137	Q,E	45.2	-	45.2	45.1	45.1	<39.1	<30.	-0.5
69	1534+580,PG	0.03	Q,P	44.3	-	44.1	44.2	44.5	38.5	90.	-0.81
70	1535+547,PG	0.038	Q	44.5	-	44.4	44.5	44.6	38.1	100.	-0.5
71	1543+489,PG	0.4	Q,P	45.9	-	46.1	45.8	45.7	40.2	60.	-0.5
72	1545+210,PG,3C323.2	0.266	L,S,D	45.8	45.8	45.8	45.9	45.9	41.7	4.	-0.98
73	1552+085,PG	0.119	Q,E	45.	44.9	45.1	45.1	44.8	<38.9	<40.	-0.5
74	1612+261,PG	0.131	Q,E	45.3	-	45.2	45.2	45.6	39.7	30.	-0.5
75	1613+658,PG*	0.129	Q,E	45.5	45.5	45.4	45.3	45.4	39.3	30.	-0.45
76	1617+175,PG	0.114	Q,E	45.2	-	45.3	45.2	45.3	<39.4	<50.	-0.5
77	1626+554,PG	0.133	Q,P	45.1	-	45.1	45.1	45.2	38.7	90.	-0.5
78	1700+518,PG	0.292	Q,E	46.	45.9	46.1	46.2	45.9	40.4	20.	-0.86
79	1704+608,PG	0.371	L,S,D	46.	-	46.1	46.2	45.8	41.1	0.5	-0.84
80	2112+059,PG	0.466	Q,P	46.5	-	46.5	46.5	46.5	40.3	70.	-0.5
81	2130+099,PG,IIZw 136	0.062	Q,E	45.2	45.4	45.1	44.9	45.	38.9	40.	-0.51
82	2209+184,PG	0.07	L,F,V	44.9	-	44.7	44.9	45.	41.2	100.	0.15
83	2214+139,PG	0.067	Q	45.	-	45.	45.	45.	38.3	100.	-0.5
84	2233+134,PG	0.325	Q,E	45.7	-	46.	45.7	45.5	39.7	60.	-0.5
85	2251+113,PG	0.323	L,S,D	45.9	45.8	45.9	46.1	46.1	41.5	3.	-0.72
86	2304+042,PG	0.042	Q,P	44.4	-	44.4	44.3	44.4	38.4	100.	-0.5
87	2308+098,PG	0.432	L,S,D	46.1	-	46.2	46.1	46.1	42.2	20.	-0.89

(Table 1 continued.)

#	name	z	class	$L_{\rm disk}$	$L_{\rm disk}$ UV	Mb	Mv	lines	Radio at 5 GHz νL_ν	$f_{\rm c}$(%)	α
88	0044+030,PG	0.624	L,S	46.6	-	46.6	-	-	42.1	40.	-0.82
89	0117+213,PG	1.49	Q	47.3	-	47.3	-	-	<40.5	<60.	-0.5
90	0946+301,PG	1.22	Q	47.1	47.1	47.1	-	-	<40.1	<70.	-0.5
91	1008+133,PG†	1.29	Q	47.3	47.7	46.3	-	-	<40.2	<70.	-0.5
92	1115+080,PG	1.72	Q	47.6	47.6	47.5	-	-	<40.3	<60.	-0.5
93	1138+040,PG	1.88	Q	47.4	47.4	-	-	-	<40.3	<60.	-0.5
94	1148+549,PG	0.969	Q	47.1	47.2	47.	-	-	40.7	40.	-0.5
95	1206+459,PG†	1.16	Q	45.6	45.1	47.2	-	-	<40.	<70.	-0.5
96	1222+228,PG,TON 1530	2.05	Q	47.6	47.5	47.7	-	-	42.2	50.	-0.5
97	1241+176,PG	1.27	L,S/F	47.2	47.2	47.4	-	-	43.2	50.	-0.50
98	1247+267,PG	2.04	Q	47.8	47.9	47.7	-	-	41.1	40.	-0.5
99	1248+401,PG	1.03	Q	46.9	46.9	46.9	-	-	<40.1	<70.	-0.5
100	1254+047,PG	1.02	Q	47.	47.	47.	-	-	40.3	70.	-0.5
101	1329+412,PG	1.93	Q	47.2	47.2	47.4	-	-	40.5	50.	-0.5
102	1333+176,PG	0.554	L,?	46.6	-	46.6	-	-	41.9	80.	-0.5
103	1338+416,PG	1.22	Q	47.3	47.3	47.1	-	-	<40.1	<70.	-0.5
104	1352+011,PG*	1.12	Q	47.2	47.2	47.	-	-	<40.1	<70.	-0.5
105	1407+265,PG	0.944	Q	47.	47.	-	-	-	41.3	30.	-0.5
106	1522+101,PG*	1.32	Q	47.7	47.9	47.3	-	-	40.4	60.	-0.5
107	1538+477,PG	0.77	L,S	46.7	-	46.7	-	-	42.1	40.	-1.
108	1630+377,PG	1.47	Q	47.4	47.4	47.3	-	-	<40.2	<60.	-0.5
109	1634+706,PG*	1.33	Q	47.9	48.	47.6	-	-	41.1	40.	-0.5
110	1715+53,PG	1.92	Q	47.4	-	47.4	-	-	40.9	40.	-0.5
111	1718+481,PG	1.08	L	47.5	47.5	47.3	-	-	42.9	50.	-0.5
112	2302+029,PG*	1.04	Q	47.2	47.3	47.	-	-	40.2	40.	-0.5
113	2344+092,PG	0.677	L,F,V	46.4	46.3	46.6	-	-	43.8	90.	-0.18
114	0134+329,3C48	0.367	L,S	45.7	45.7	-	-	-	41.8	0.5	-0.94
115	0232−042,PHL1377*	1.44	L,S	47.3	47.3	-	-	-	43.4	20.	-0.77
116	0237−233,PKS,MRC	2.22	L,S	47.5	47.5	-	-	-	<43.8	<5.	-0.15
117	0405−123,PKS	0.574	L,S	46.9	46.9	-	-	-	<43.2	<20.	-0.52
118	0414−060,3C110	0.781	L,S	46.6	46.6	-	-	-	42.4	10.	-0.75
119	0710+458,Mkn376	0.056	Q	44.4	44.4	-	-	-	39.	7.	-0.5
120	0742+318,4C31.30	0.462	L,F	46.3	46.3	-	-	-	43.3	70.	-0.23
121	0906+484*	0.118	Q	45.6	45.6	-	-	-	<39.	<90.	-0.5
122	0955+326,3C232	0.533	L,S	46.2	46.2	-	-	-	42.6	10.	-0.53
123	0958+551,Mkn132	1.76	Q	47.7	47.7	-	-	-	<41.5	<40.	-0.5
124	1011+250,Ton490	1.63	L,F,V	46.9	46.9	-	-	-	43.9	100.	0.34
125	1317+277,Ton153	1.02	Q	47.	47.	-	-	-	<40.6	<70.	-0.5
126	1421+330,Mkn679	1.9	Q	47.4	47.4	-	-	-	41.7	40.	-0.5
127	1435+638	2.06	L,F,V	47.4	47.4	-	-	-	44.2	80.	-0.17
128	1821+643,E1821+643	0.297	Q	46.6	-	46.6	-	-	41.1	60.	-0.5
129	2041−109,Mkn509*	0.036	Q	45.	45.	-	-	-	38.8	30.	-0.56
130	2145+067,4C06.69	0.99	L,F,V	46.8	46.8	-	-	-	44.4	100.	0.029
131	2201+315,4C31.63	0.297	L,F,V	46.1	46.1	-	-	-	43.4	80.	-0.025

(Table 1 continued. The extended sample.)

#	name	z	$L_{\rm disk}$	Radio at 5 GHz		
			$f \cdot Q_{\rm jet}$	νL_ν(core)	$f_{\rm c}(\%)$	α
132	0106+13,3C33	0.059	45.4	40.2	0.6	-0.77
133	0109+49,3C35.0	0.066	44.4	40.1	2.	-0.85
134	0152+28,3C42	0.395	45.9	40.8	0.2	-0.9
135	0132+37,3C46	0.437	46.	40.7	0.5	-0.87
136	0221+27,3C67	0.31	45.7	42.6	20.	-0.91
137	0307+16,3C79	0.255	46.2	41.	0.6	-1.1
138	0356+10,3C98	0.03	44.9	39.2	0.2	-0.65
139	0410+11,3C109	0.307	46.2	42.6	20.	-0.7
140	0411+14,4C14.11	0.38	45.1	41.7	2.	-0.77
141	0433+29,3C123	0.218	46.1	42.	0.6	-0.89
142	0702+74,3C173.1	0.292	46.1	41.	0.7	-1.
143	0734+80,3C184.1	0.119	45.	40.2	0.5	-1.3
144	0745+56,4C+56.16	0.035	44.4	40.7	20.	-0.98
145	0802+24,3C192	0.06	45.1	39.6	0.3	-0.69
146	0917+45,3C219	0.174	45.4	41.4	2.	-1.
147	0936+36,3C223	0.137	45.7	40.5	0.7	-0.78
148	0944+73,4C73.08	0.058	45.2	40.1	3.	-0.93
149	0958+29,3C234	0.185	45.9	41.9	7.	-0.97
150	1003+35,3C236	0.099	45.4	41.9	30.	-0.65
151	1030+35,3C244.1	0.428	45.9	$<$40.2	$<$0.04	-1.
152	1308+27,3C284	0.239	45.4	40.5	0.7	-1.1
153	1319+42,3C285	0.08	44.4	39.9	0.8	-0.82
154	1409+52,3C295	0.461	46.2	41.4	0.1	-1.1
155	1420+19,3C300	0.27	45.4	40.9	0.5	-0.99
156	1441+52,3C303	0.141	45.1	41.7	10.	-0.61
157	1522+54,3C319	0.192	45.	$<$39.8	$<$0.1	-1.
158	1529+24,3C321	0.096	45.4	40.7	2.	-0.92
159	1550+20,3C326	0.098	45.4	40.4	3.	-2.1
160	1626+27,3C341	0.448	46.7	40.3	0.1	-1.
161	1658+47,3C349	0.205	45.7	41.2	2.	-0.81
162	1832+47,3C381	0.161	45.7	40.4	0.3	-0.8
163	1833+32,3C382	0.058	44.9	41.1	9.	-0.65
164	1842+45,3C388	0.092	44.9	41.	3.	-0.93
165	1845+79,3C390.3	0.057	45.1	41.3	8.	-0.87
166	1939+60,3C401	0.201	45.4	41.4	2.	-1.
167	2141+27,3C436	0.215	45.4	41.1	1.	-1.
168	2153+37,3C438	0.29	45.9	41.1	0.4	-1.2
169	2243+39,3C452	0.082	45.2	41.2	4.	-0.87
170	2309+18,3C457	0.31	46.4	40.6	0.5	-0.91

Table 2: The FR II sample used in this paper. Col. (1): ID number, Col (2): IAU name; Col. (3): redshift, Col. (4): disk luminosity, derived by multiplying the lobe power calculated by RS91 with a factor 10; Col. (5): radio luminosity of the core at 5 GHz rest frame, Col. (6): ratio of core flux to total flux at 5 GHz rest frame in per cent; Col. (7): differential spectral index of fitted spectrum at 5 GHz rest frame.

of the core emission in radio loud quasars comes from a very compact region on the parsec scale it is evident that the difference between radio loud and radio weak quasars is established already at this small scale.

Finally we note that radio loud quasars with lobe emission (morphologically similar to FR II radio galaxies) exist only at disk luminosities $L_{\rm disk} \geq 10^{46}$ erg/sec although radio weak sources with 100 times lower accretion rate do exist in large numbers. Unless there is a strange selection effect – this is an optically selected sample – it means that disks must have luminosities larger than a threshhold luminosity of $\sim 10^{46}$ erg/sec to produce a quasar with FR II type radio jet.

5 Confronting theory with data

5.1 Scaling with disk luminosity and velocity

What kind of correlation do we expect between radio core and UV emission? If we base our answer on the idea of a jet-disk symbiosis than we find from *Paper I* that for a statistical sample the radio flux scales with disk luminosity, bulk Lorentz factor $\gamma_{\rm j}$, and Doppler factor $\mathcal{D}$ as

$$F(\text{radio core}) \propto \mathcal{D}^{2.2} \gamma_{\rm j}^{-1.8} L_{\rm disk}^{1.42} \tag{10}$$

for radio loud and radio weak quasars.

There are a few more parameters involved like the relativistic electron number density $x_{\rm e}$ in units of the total (proton) particle density and the mimimum energy of the electrons $\gamma_{{\rm min},e} m_{\rm e} c^2$, the total jet power $q_{\rm j/l}$ normalized to the disk luminosity and the inclination angle i. For homogenous classes of objects we assume that all these parameters will scatter around a constant value. This will lead to a certain scatter of the radio luminosity around an average value. To simplify the analysis we will, however, assume that the dominant reason for scattering will be the randomly oriented inclination angle with the consequence of strong Doppler boosting. This can lead to a broadening of the distribution by a factor 10-100 (see Fig.3). The assumption now is that the scatter introduced by the other parameters is less than this in the regime of relativistic flows. If this is too much a simplification and the broadening of the distribution is caused by intrinsic parameter variations than the average bulk Lorentz factors we derive here have to be regarded as upper limits. This, however, seems unlikely as the Lorentz factors of 3-10 we obtain are quite consistent with many other studies in the past (eg. Ghisellini et al. 1993).

In the earlier discussions on the nature of the quasar radio emission it was suggested that relativistic beaming was responsible for the scatter of all quasars (radio loud and radio weak) but as Strittmatter et al. (1980) showed this is inconsistent with the flux density distribution of optically selected quasar samples and there is a real dichotomy in the radio flux. Hence, we suggest that the scatter within each population is dominated by relativistic boosting and there is an additional discrete process producing an offset between radio loud and radio weak.

The scaling over several orders of magnitudes in the radio luminosity thus will reflect mainly the change in the accretion rate which indeed may vary over 4 orders of magnitudes in the quasars alone and even more if one later includes Seyfert galaxies and stellar mass black holes. The non-linearity between disk luminosity and radio flux is a consequence of the non-linear response of the synchrotron emissivity to a change in the magnetic energy density. Nevertheless, there still remains one uncertainty in the discussion of the scaling, namely, we have no idea whether the jet velocity also depends on the mass accretion rate. We only can argue that this dependence is not very strong because the observed Lorentz factors in jets are usually estimated to be in the range 3-30 (Ghisellini et al. 1993) with a mean value of ~ 10, despite a large range of mass accretion rates of at least 2 orders of magnitudes for radio loud quasars. One could also argue that the escape velocity around black holes is a substantial fraction of the speed of light, so that jets with speed $\ll 0.5c$ from black holes are difficult to achieve unless there is a perfect fine-tuning in the acceleration mechanism. On the other hand will the Compton drag of disk photons decelerate the jet if it starts at $\gamma_{\rm j} \gg 10$ (Melia & Königl 1989). In light of this discussion we make the Ansatz that the bulk proper velocity of the jet depends on the accretion rate and thus on the disk luminosity in the quasar luminosity range[1] as

$$\gamma_{\rm j}\beta_{\rm j} = \gamma_{\rm j,0}\beta_{\rm j,0} \left(\frac{L_{\rm disk}}{10^{46}{\rm erg/sec}} \right)^{\xi} \tag{11}$$

[1] One should understand this scaling in statistical terms. If the jet velocity depends on the ratio $L_{\rm disk}/L_{\rm edd}$ and the average of this ratio has a slight dependence on the total power (see SM89) this could produce such a scaling indirectly.

with the additional assumption that for quasars $|\xi|$ is a small number (< 0.5), $\beta_{\rm j,0} \simeq 1$ and $\beta_{\rm j} \simeq 1$ (see above). Following our general philosophy that disks and jets are basically the same everywhere we assume the same scaling for radio weak quasars.

5.2 Obscuring dust torus

The PG quasars we use are selected by their blue color and not by their radio flux. In our context this part of the spectrum is produced by the accretion disk and should be relatively free of any substantial selection effect like boosting. We only have to take into account that an obscuring dust torus surrounding the nucleus could prevent us from seeing edge on disks. This, on the other hand, is even helpful because the disk luminosity is then even less dependent on the inclination angle if we deal with maximally rotating black holes as central objects (Cunningham 1975): light bending and a moderate amount of boosting due to the high rotational velocity compensate the effects of decreasing apparent surface with higher inclination angles.

It is not really known what the real opening angle of the viewing cone permitted by the torus for each quasar population is and it might iself depend on other parameters (i.e. jet power and z, see Kapahi 1990, Falcke et al. 1994). We pick for the assumed obscuring dust torus of radio weak quasars deliberately a viewing cone with semi-opening angle of 60° – saying that we do not detect 50% of the quasars because of obscuration – and obtain as an average inclination angle for the jet axis with respect to the line of sight in this sample $i \approx 40°$. In the range $60° > i > 18°$ we should find 90% of our sample. This value for the obscuring torus is taken from McLeod & Rieke (1994) who investigated the host galaxies of a subsample of the PG quasars.

Studies of the ratio between FR II galaxies and radio loud quasars suggest that this torus might there even cover a larger area than for radio weak quasars and we take 45° as a default value (Barthel 1989). Which means, we miss more than 2/3 of all sources and the 90% dividing line is at 14°. None of our conclusions depends sensitively on these assumptions and we will later show that those numbers are able to explain the UV-radio correlation in a consistent manner.

5.3 Parameter space for radio loud jets

We now discuss the range of parameters needed to explain the UV-radio correlation as being due to a link between jet and disk. In *Paper I* we presented the most simple minded model for the jet emission and its parameters and noted that in order to explain the high radio flux of radio loud cores we get close to the limits imposed by energy and mass conservation in a jet-disk system. We will fit the model step by step to the data and discuss the range of possible parameters. Among all possible models only the most efficient case, a 'total equipartition jet' — implying rough equipartition between energy stored in magnetic field, electrons and protons and bulk kinetic motion — is able to explain these radio fluxes. Let us now first fix the plasma parameters of this type of jet such that they yield maximum efficiency (see *Paper I*) which implies:

a) a minimum Lorentz factor of the relativistic electron distribution of $\gamma_{\rm e} \approx 100$ for a powerlaw distribution with $p = 2$,

b) a relativistic electron fraction $x_{\rm e} \approx 1$ which means that in a proton/electron jet all electrons get accelerated or that for every thermal electron one additional secondary particle (electron or positron) is created and

c) a proton/electron ratio of $\mu_{\rm p/e} \approx 2$ meaning equal energy in relativistic proton and electron distribution ($u_3 \approx k_{\rm e+p} \approx 1$ and $\ln(\gamma_{\rm e,max}/\gamma_{\rm e,min}) \approx 3.6$)

According to the discussion in *Paper I* one may vary some of these 'microscopic' parameters but there is no way to further increase the emitted flux of the jet other than by changing the 'macroscopic' parameters which are

a) the jet Lorentz factor $\gamma_{\rm j}$, assumed to be of the order 10 ($\Rightarrow \beta_{\rm j} = 1$),

b) the disk luminosity L_{46} in units of 10^{46} erg/sec which varies in our sample from 10^{-2} to 10^{2} and

c) the total jet power $q_{\rm j/l}$ in units of the disk luminosity which we consider to be < 1.

These parameters are fixed initially at these extreme values only to formally describe the radiatively most efficient state of the jet but they are not necessarily unphysical. For example if the electrons responsible for the synchrotron emission are secondary pairs created in hadronic cascades than a low energy cut-off at $\gamma_{\rm e} \geq 180$ is a natural consequence of the Pion decay and because one is not limited by the number of thermal plasma electrons (as in a pure shock acceleration scenario for the electrons) the ratio $x_{\rm e}$ of relativistic to thermal electrons may be

very high. The product $x_{\rm e}\gamma_{\rm e,min}$ is then only limited by the total energy constraints. When the parameters are fixed in this way and one calculates the emitted flux for a supersonically expanding jet with maximal internal energy contents one gets (*Paper I*)

$$\begin{aligned}\nu L_\nu(5{\rm GHz}) &= 6.7\cdot 10^{42}\,{\rm erg/sec}\,\mathcal{D}(L_{46},i_{\rm obs})^{2.17}\sin i_{\rm obs}^{0.17}\\ &\cdot\left(\frac{\gamma_{\rm e,min}x_{\rm e}}{100}\right)^{0.83}\left(\frac{6}{\gamma_{\rm j,0}}\right)^{1.8} q_{\rm j/l}^{1.42}L_{46}^{1.42-\xi}.\end{aligned} \tag{12}$$

where we have already made use of the possible velocity scaling (Eq. 11) and the parameter setting discussed above. The Doppler factor $\mathcal{D}$ is defined as

$$\mathcal{D} = 1/\gamma_{\rm j}(1-\beta_{\rm j}\cos i_{\rm obs}). \tag{13}$$

For our comparison with the data we will assume that all jets are two-sided.

In order to fix the parameters we first try to fit the cores of the lobe dominated radio loud quasars at $L_{\rm disk}\simeq 10^{46}$ erg/sec and find that already there the possible parameter range is very narrow. The quasars can not be fitted with bulk Lorentz factors $\gamma_{\rm j,0}\geq 10$ and $q_{\rm j/l}<1$ as with increasing Lorentz factor the radiative efficieny is decreased and the boosting effect reduces the visible radio flux for the bulk of the population even further. Together this makes a very strong effect which depends on the Lorentz factor roughly as $\gamma_{\rm j,0}^{-4}$.

We also can get an approximate lower limit for the Lorentz factor from our prerequisite that the width of the distribution is mainly given by the scatter in inclination angles. A small Lorentz factor would yield only a narrow band for the scattering width of the UV-radio correlation and some sources would fall outside this band so we conclude that $\gamma_{\rm j,0}\geq 3$ ($q_{\rm j/l}\geq 0.05$). The width (and therefore the scattering) of the radio flux distribution is represented in Fig. 3 by grey lanes. Quasars with larger inclination angle (below the lane) are assumed to be missing in our sample due to an obscuring dust torus and smaller inclination angles (above the lane) will lead to a strong boosting effect hence $\sim 10\%$ of each sample should lie close to or above this lane.

In a second step we include the remaining sources and first adopt the velocity gradient by varying ξ in Equation (11). As noted before the gradient must not be very steep because of the fourth power entering in Equation (12); this is highlighted in Fig. 3 where we show the expected UV-radio correlation for ξ as large as 0.5. It is not possible to determine this evolution in more detail from the few radio loud sources in our sample, especially as the high power sources do not belong to the well defined subsample of PG quasars with $z<0.5$. We only can hope that the distribution of the high power sources is not completely misleading and estimate that $0\leq\xi\leq 0.25$.

Finally we include the CDQ in our analysis. A strict upper limit of the radio flux as a function of disk luminosity is given by those models with maximum boosting ($i=0$) and no source in our diagram should be far above this line. This condition gives us additional limits on the Lorentz factor and also ξ. Moreover should most of the CDQ cluster around a line representing sources at the boosting cone thus inclined to line of sight by $i\simeq 1/\gamma_{\rm j}$. This restricts the margins for the Lorentz factor even further. Figure 3 shows different parameter combinations and our best fit model with estimated errors.

$$\gamma_{\rm j}=6^{+2}_{-2},\ q_{\rm j/l}=0.15^{+.2}_{-.1},\ \xi=0.15^{+0.1}_{-0.15} \tag{14}$$

The best fit parameter set implies that indeed the microphysical state of the plasma must not be too far away from the radiatively most efficient state, i.e. $x_{\rm e}\gamma_{\rm min,e}\approx 100$, otherwise we will have to increase $q_{\rm j/l}$ substantially. Accordingly we have an indirect argument that the electron distribution in radio loud quasars either must have a low energy cut-off or consists of additionally created pairs. We suggested in *Paper I* that both effects might naturally arise if the electron population is dominated by pairs produced in the $\pi-$decay of hadronic cascades initiated by pp or $p\gamma$ collisions.

5.4 Applying the parameters to radio weak jets

As discussed in *Paper I* we proposed to test if the radio emission from radio weak sources could be explained with emission from jets similar to those observed in radio loud quasars. Based on the idea that quasars are all powered by accretion disks around black holes, it is hard to understand how the jet production in the accretion disk very close to the black hole ($\ll 1$ pc) should depend on environmental effects (e.g. type of galaxy). We noted that a difference in the efficiency of electron acceleration (e.g. production of secondary pairs) could naturally account for the different radio luminosities. The acceleration of these electrons must happen at a larger scale (≥ 1 pc) because of strong synchrotron losses further in, and might well be triggered by environmental effects (e.g.

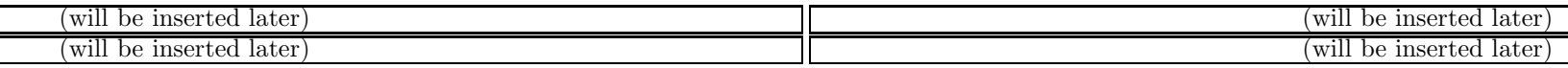

Figure 3: Different Models for the UV-radio correlation (Fig. 2) for different Lorentz factors $\gamma_{\rm j,0}$ and velocity evolution power index ξ. The jet power $q_{\rm j/l}$ is adjusted such that the bulk of radio loud quasars at $L_{\rm disk} = 10^{46}$ erg/sec are always fit. Upper lane: 'total equipartition' jet. Lower lane: 'protonic' jet. The widths of the grey lanes is given by different inclination angle. Dashed line: Boosted sources with $i = 1/\gamma_{\rm j}$. Solid line: Maximum possible boosting ($i = 0$). From top left to bottom right we have: (a) Best fit: $\gamma_{\rm j} = 6$, ($q_{\rm j/l} = 0.15$), $\xi = 0.15$. (b) Lorentz factor too high: $\gamma_{\rm j} = 10$, ($q_{\rm j/l} = 1$), $\xi = 0$ (CDQ are too low). (c) Lorentz factor too low: $q_{\rm j/l} = 0.025$, $\gamma_{\rm j} = 2.5$, $\xi = 0.15$ (CDQ too high and distribution too narrow). (d) Velocity evolution too strong: $\gamma_{\rm j} = 6$, ($q_{\rm j/l} = 0.15$), $\xi = 0.5$.

interaction between jet and ISM in a shear layer). But as radio weak quasars, unlike their radio loud siblings, do not all populate the extreme parts of the parameter space, observations are not yet able to decide what is the real distinction between radio loud and radio weak. In *Paper I* we suggested at least another 3 alternative scenarios. For the discussion in this Paper we will confine our attention only to the case of a 'protonic' jet (**BP** model in *Paper I*). Nevertheless, all other proposed models would yield similar results; only the interpretation of the microscopic parameters would change.

The protonic jet is obtained by increasing the relativistic proton/electron ratio $\mu_{\rm p/e}$ by a factor 100 which means we reduce the energy stored in relativistic electrons by the same factor, but leave everything else in the jet unchanged. The magnetic field would still be in equipartition with relativistic particles, namely the protons, and both still constitute a major fraction ($\sim 50\%$) of the total jet power (the other half is in kinetic motion). The value for $\mu_{\rm p/e}$ is not ad-hoc but a natural configuration in cases where all electrons are accelerated from their thermal distribution ($x_{\rm e} \simeq 1$) into a powerlaw distribution starting at $\gamma_{\rm e,min} \approx 1$. From *Paper I* we obtain as the core luminosity

$$\begin{aligned} \nu L_\nu(5{\rm GHz}) &= 1.0 \cdot 10^{41}\,{\rm erg/sec}\,\mathcal{D}(L_{46}, i_{\rm obs})^{2.17} \sin i_{\rm obs}^{0.17} \\ &\quad \cdot (\gamma_{\rm e,min} x_{\rm e})^{0.83} \left(\frac{6}{\gamma_{\rm j,0}}\right)^{1.8} q_{\rm j/l}^{1.42} L_{46}^{1.42-\xi}. \end{aligned} \tag{15}$$

There is no way to definitively prove this notion, but we could easily falsify it. We just take the parameters derived for radio loud jets, apply them to Eq.(15) and insert this in our diagram without further fitting. The lower bands in Figure 3 represent the protonic jet model where we only have changed the proton/electron ratio by a factor 100 and the opening angles of the torus to 60° to be consistent with other findings as discussed before. The agreement is surprisingly good and indeed we can easily match all three populations (CDQ, LDQ, radio weak quasars) with a single model where the difference is only due to relativistic boosting and different relativistic electron populations.

We have to comment on one additional effect seen in this data. There seems to be a slight curvature in the radio weak population towards high powers. Unlike the case for the extended emission, there is no reason to suppose that any kind of cosmological evolution in this diagram would produce that effect. The core luminosity depends only on the accretion rate and not on the environment. A change in the accretion rate with z should shift a quasar only parallel to the distribution. Strong evolution effects in this diagram would be a serious argument to falsify our theoretical understanding of the radio core. However, the curvature is only minimal and could easily be caused by technical or selection effects, especially as this curvature is mainly seen in the high redshift PG sample where strong selection effect are known to exist (Wampler & Ponz 1985). Should selection effects not be the main cause for this curvature one might argue that this is indeed a sign of a velocity gradient index $\xi \neq 0$, but this is the only indication, and still $\xi = 0$ gives a good approximation to the data. One may test this in the future by incorporating larger complete samples for radio loud and radio weak quasars with high powers.

5.5 RIQ: Boosted radio weak quasars?

One inevitable consequence of our "relativistic jets in all quasars" hypothesis is that a fair fraction of all radio weak quasars are boosted and appear as radio loud quasars. For the following discussion we only refer to the PG sample with $z < 0.5$ if not stated otherwise.

The cores of the 11 steep spectrum LDQ appear as radio loud, these quasars obviously form a separate subclass, which is physically different from radio weak quasars already in the cores. The rest of 5 objects, however, is a possible sample of beamed radio weak quasars, because they show all characteristics one might expect from a boosted source: strong compact core, high variability and flat spectrum. Two of them (PG 1226+023 and PG 1302−102) show a lobe structure themselves and therefore are likely to be boosted specimen of radio loud quasars whereas the remaining 3 objects (PG 0007+106, PG 1309+355, PG 2209+184) apparently do not show any extension and are candidates for boosted radio weak quasars. We use these sources to define a subclass of radio quasars, the radio-intermediate quasars (RIQ). To be classified as such we demand a variable flat spectrum compact core without a large scale lobe structure that in a UV-radio core diagram are found among, or on the extrapolation of, the cores of LDQ. Two other candidates for this kind of sources are PG 1351+640 and PG 1333+176 (see Notes).

We have now three independent means to check the idea that RIQ are boosted radio weak quasars: the number of beamed sources, the offset between boosted and normal quasars and the emission line characteristics.

a) The ratio of the number of boosted to non-boosted objects reflects the angle of the boosting cone which is $\arcsin 1/\gamma_{\rm j}$. For a sample of N objects with a boosting cone of $1/\gamma_{\rm j}$ and an obscuring dust torus with semi-opening angle of $\phi_{\rm torus}$ we expect

$$n = N\,(1 - \cos \arcsin\,(1/\gamma_{\rm j}))\,/\,\cos\,\phi_{\rm torus} \tag{16}$$

strongly boosted objects. Here we have $N = 73$, $n = 3 \pm 1.7$ and assume $\phi_{\rm torus} \simeq 60^\circ$ which corresponds to a γ-factor for the jet of $\gamma_{\rm j} = 5^{+2.7}_{-1}$. Inclusion of the fourth source will reduce this value slightly.

b) The offset of the boosted from the non-boosted population is a function of the Doppler factor as well. Alas, despite the major popoulation being called 'non-boosted' it is still affected by boosting and we do not know exactly what the average inclination angle of our sample really is, as we obviously have only upper limits in the high inclination part of our diagram. We first fit a straight line with *fixed slope* to both populations. The 3 boosting candidates are a factor 153 more luminous in the radio. Using the Doppler factors from our model, we find γ-factors in the range $\gamma_{\rm j} = 1.7$ to $\gamma_{\rm j} = 4.8$ for the range of inclination angles $(60^\circ - 20^\circ)$ we attribute to the bulk of our parent population. Here we assumed that all boosted jets show no inclination to the line of sight; a more reasonable value for the inclination angle will lead to slightly higher values of $\gamma_{\rm j}$. In Fig 3 the area between the lower pair of dashed and full line represents the expected region for boosted-radio weak quasars, for the parameter set discussed before. Indeed, taking the uncertainties into account, the RIQ are compatible with this model prediction. Of course, an association with the extrapolation of the radio loud CDQ is not completely excluded but is less likely.

c) BG92 found one significant emission line indicator, which separated radio loud from radio quiet objects in so far that radio loud objects show almost no evidence for Fe II emission lines, whereas radio weak quasars do. Our sample of suspected boosted radio weak quasars clearly shows enhanced level of Fe II emission, in agreement with being radio weak, in marked contrast to the double lobe sample which shows no significant FeII emission. In addition there are some other differences between radio loud and radio quiet and taking all together BG92 come to the conclusion that the sample of flat spectrum sources has emission properties like radio quiet quasars but unlike radio loud quasars.

The hypothesis of boosted radio weak quasars passed all three tests reasonably well. Both estimates for the Lorentz factor are in agreement with each other and our previous estimate and support the hypothesis of having relativistic jets in radio weak quasars.

5.6 FIR emission

Another consequence of having jet emission in radio weak quasars is the possibility to see this emission at higher frequencies. In *Paper I* we showed that we can expect non-thermal emission in the rest frame up into the submm regime. Unfortunately the expected flux is on the mJy level which is difficult to observe with current detectors. Chini et al. (1989) observed a subsample of the PG quasars at 230 GHz, showing that the IR emission at higher frequencies in quasars is of thermal origin. They detected only 5 quasars at 230 GHz and concluded from the spectrum that the emission up to this frequency is non-thermal while beyond 230 GHz thermal dust emission takes over. We give a table of spectral indices α between these fluxes and the 5 GHz VLA core and total fluxes (except for 2041−109 where we take the flux referenced in Chini et al. 1989) of the 5 objects being in our extended sample. We define the spectral index to be positive for inverted spectra ($F_\nu \propto \nu^\alpha$).

All spectral indices are flat or inverted as expected if there indeed is a strong flat (inverted) spectrum core. In our picture the non-thermal emission at this frequency should come from a very small region of the order

Table 3: High frequency spectral indices for radio weak quasars detected at 1.3 mm: $\alpha_{\rm core}$ is the spectral index between the coreflux at 6 cm and the total flux at 1.3 mm while $\alpha_{\rm total}$ is the spectral index between the total flux at 6 cm and 1.3 mm.

Name	$F_{230\rm GHz}[mJy]$	$\alpha_{\rm core}$	$\alpha_{\rm total}$
0007+106	3.9 ± 1	$0.51^{+0.06}_{-0.08}$	$0.48^{+0.06}_{-0.08}$
1411+44	3.9 ± 1	$0.51^{+0.06}_{-0.08}$	$0.48^{+0.06}_{-0.08}$
2041–10	4.0 ± 1	–	$-0.08^{+0.05}_{-0.08}$
2130+09	2.1 ± 0.7	$0.23^{+0.08}_{-0.1}$	$0.01^{+0.08}_{-0.1}$
2214+13	3.5 ± 0.6	–	$0.7^{+0.04}_{-0.05}$

10^{17} cm away from the disk and therefore we are allowed to peek into the region where the jet establishes itself and may still be in a state of accelerating its inital electron population. Interestingly the Galactic Center source Sgr A* shows a similar inverted spectrum in the mm to submm range where we explained this qualitatively as being radiation coming from the jet nozzle (FMB, Falcke & Biermann 1994a, Falcke 1994b).

6 Unification with FR II galaxies

6.1 Estimating the hidden disk luminosity

An often used assumption is that FR II radio galaxies and quasars are basically the same objects but seen at different inclination angles (Barthel 1989). Seen edge on, the obscuring dust torus will prevent us from observing UV-bump and broad line region and we cannot classify the radio source as a quasar. In fact, if an obscuring dust torus is indeed present, and the widths of the lanes in Fig. 3 do support such a concept, the separation between quasars and radio galaxies is a necessary consequence.

In the following we will assume that the unification scheme is correct and that FR II galaxies and radio loud quasars are identical except for different inclination angles. This implies the presence of an accretion disk in FR II radio galaxies like in quasars and we would expect that inserted in our radio/$L_{\rm disk}$ diagram the cores of FR II radio galaxies should occupy a region slightly below the radio loud quasars – because of less boosting – while the total (lobe) emission radio galaxies and quasars should occupy exactly the same region. For testing this we will make use of the sample of radio selected FR II galaxies used by RS91.

A big problem of the sources in this sample is that per definition it is almost impossible to measure their disk luminosity. Rawlings et al. (1989) tried to use the OIII narrow line as an indicator but found only weak correlations. Later RS91 used a combination of different narrow lines to obtain a better indicator for the central luminosity and indeed found a good correlation between the luminosity of these lines and the power stored in the radio lobes divided by the age of the lobe – the total jet power. Unfortunately, they did not tabulate these narrow line luminosities, and anyway it would be difficult to calibrate such an indicator to an absolute value of the disk luminosity as we did for our sample.

Hence, we are not able to construct a real radio/$L_{\rm disk}$ diagram for FR II radio galaxies and prove any optical/radio correlation. Nevertheless, we can use the knowledge gained in this paper to perform an important consistency check of our results. The idea, we have followed throughout this paper, is that the average ratio between jet power and disk luminosity is constant within our sample. Given that the unification scheme and the value $Q_{\rm jet}/L_{\rm disk}$ we have derived is correct we can now turn the argument around and estimate the hidden disk luminosity of FR II radio galaxies from the jet power. For this we take the jet power $Q_{\rm jet,RS91}$ derived by RS91 and correct their minimum energy estimates by a factor $f_{\rm RB93} \sim 3$ for the presence of relativistic protons. Rachen & Biermann (1993, RB93) and Rachen et al. (1993) investigated the extragalactic ultra-high energy tail of the cosmic ray population, which is most likely to stem from radio lobes, and found that the cosmic ray ratio in hotspots of FR II galaxies should be of the order 20 which yields a factor 3 increase for the derived total jet power. Thus we obtain as a conversion formula

$$L_{\rm disk} = 10\, Q_{\rm jet,RS91} \left(\frac{f_{\rm RB93}}{3}\right) \left(\frac{q_{\rm j/l}}{0.15}\right)^{-1}. \qquad (17)$$

Figure 4: Monochromatic luminosity of the compact radio core versus the disk luminosity (see text) for radio loud quasars with (circles and boxes – see Fig. 2) and FR II galaxies with $z < 0.5$ (crosses) . The 'disk luminosity' for FR II galaxies was obtained by applying a general conversion factor $L_{\rm disk} = 10 Q_{\rm jet}$ to their lobe energies estimated by RS91. The shaded band gives our radio loud model for inclination angles of 15° to 45°. The lower grey line is the extension of the band for 90° inclination.

where a factor $2q_{\rm j/l}$ accounts for the two-sidedness of the jets.

6.2 Core emission

Now we can use the hidden disk luminosity Eq.(17), proceed as before, and plot radio core luminosities versus disk luminosity. We used the core fluxes listed in Rawlings et al. (1989) and total fluxes from the NED database and converted them into the rest frame just the way we did for quasars.

With the conversion factor $q_{\rm j/l} = 0.15$ and $f_{\rm RB93} = 3$ we reproduced our diagram in Fig. 4 for the radio loud sources only, where small crosses represent the FR II cores. The theoretical 'best fit' radio loud model from Fig. 3 is redrawn and the grey line below gives the widening of the band for including up to 90° (edge-on) orientation.

The expected coincidence between FR II radio galaxies and quasars is indeed present. The overlap of these two populations was obtained without further adjusting previously constrained parameters and therefore is an independent test for several conclusions drawn before, e.g. the high jet power $2Q_{\rm jet}/L_{\rm disk} \sim 0.3$. This is also a check for the consistency of the unification theory, and we conclude from the fact that FR II galaxies occupy the anticipated region that the implied scaling of the jet cores with disk luminosity seems to be correct in quasars, as well as in FR II galaxies and that double lobed quasars and FR II galaxies have similar jet properties. A major parameter to influence the core brightness is the inclination angle, and as expected the FR II cores cluster at the lower end of the distribution, such that approximately 2/3 of the FR II cores are close to or below the 45° line of the model extending well down to the 90° line.

This effect is highlighted by the core to lobe ratio at 5 GHz (restframe) in both populations for the quasars where the median values are

$$\left\langle \frac{L_{\rm core,quasars}}{L_{\rm lobe,quasars}} \right\rangle = 15\% \qquad \left\langle \frac{L_{\rm core,FRII}}{L_{\rm lobe,FRII}} \right\rangle = 0.8\% \; . \tag{18}$$

If we exclude the two CDQ one would get 8% for the quasars, still the quasars have substantially brighter cores compared to FR II galaxies. This originally was one of the reasons to propose the quasar/FRII unification scheme. Only one of the radio cores (3C341) falls far below the theoretically expected range and one should re-examine the determination of the jet power or look for other pecularities. On the other hand this offset might only indicate the larger uncertainty in determining the hidden disk luminosity.

6.3 Extended emission

Does the coincidence of FR II and quasar fluxes also hold if one compares the extended fluxes? Figure 5 shows the total flux of all sources plotted versus the disk luminosity. FR II sources are again incorporated using the conversion parameter $2q_{\rm j/l} = 0.3$ as before. We used the total luminosity as it is in most cases dominated by the lobes and it is by far the most reliable datum we have. As the lobe emission is assumed to be unaffected by boosting we expect that the total flux of LDQ and FR II show exactly the same distribution. The fact that this is indeed the case is another independent check of the consistency of unification and of our parameter $q_{\rm j/l}$. The distribution scales with the disk luminosity and is very narrow; it scatters only by a factor 3 in both directions – much less than for the core fluxes where different inclination angles broaden the distribution. CDQ are still at the upper end of the distribution, however, they are no longer clearly separated.

We also plotted as a full line the lobe luminosity $2 \cdot L^*_{\rm lobe}$ derived in *Paper I* from extrapolating the physical situation in the core out to the lobes; the dashed lines are each offset by 0.5 in the log to indicate the scatter. Although the agreement is fairly good one should be careful with the interpretation as the derivation is very simplified (e.g. the dissipation of kinetic energy is still unclear) and serves only as an order of magnitude check.

In our sample consisting of sources with $z < 0.5$ we do not expect strong cosmological evolution, for sources with higher redshift it appears as if indeed there is a tendency for PG quasars to have lower radio flux, perhaps

(will be inserted later)

Figure 5: Monochromatic total luminosity of quasars (boxes, circles and points – see Fig. 2) and FR II galaxies (crosses). The 'disk luminosity' for FR II galaxies was obtained by applying a general conversion factor basing on our analysis to the jet powers (RS91). The radio loud quasar sticking out from the general distribution is the CSS source 3C48.

caused by cosmological evolution. Lobes of quasars at higher redshift may be relatively fainter although equally bright in absolute terms, but statistical statements seem to be problematic with this small number of sources and it is suspicious that radio loud and radio weak high redshift PG quasars seem both to be shifted to relatively lower radio emission whereas the other soures do not show this trend.

6.4 Extended emission in radio weak quasars

For the radio weak population there also is a correlation between total radio luminosity at 5 GHz and disk luminosity, but the scatter of the distribution is larger than in the radio loud quasars and slightly larger than in the cores alone. In these sources we obviously have a mixture of many contributions. A popular idea is that the diffuse emission is caused by starbursts or starburst-driven superwinds (Baum et al. 1993), but in this case starburst and AGN activity must be strongly linked by the large scale accretion flow in the galaxy to provide this correlation. The alternative explanation than is that a large fraction of the extended emission is caused by diffuse emission from the terminating or disrupting jet flow as seen in many Seyfert galaxies (e.g. NGC1275, see Böhringer et al. 1993 and refs.). This would require the jet to terminate at the kiloparsec scale, which is difficult to explain with the assumption of equal powers for jets in radio loud and radio weak quasars. One would have to favour a dichotomy in the jet production itself with a lower $Q_{\rm jet}/L_{\rm disk}$ in radio weak quasars and not a dichotomy in the electron acceleration. On the other hand radio weak quasars are mostly spirals having a completely different density profile along the rotation axis as ellipticals where radio loud quasars are found, and one might speculate that jets in spirals either terminate almost invisibly far out or very close to the center. Interestingly half of the detected radio weak quasars show no extended emission at all.

7 Summary

We used an optically selected quasar sample to test our idea that jet and disk are symbiotic features which are equally important for the overall energy budget of the AGN and are present in radio loud and radio weak quasars. From UV-bump fits we derived empirical relations between disk luminosity and other luminosity indicators (optical continuum, $M_{\rm b}$, OIII, He II and H_β). We then plotted the average disk luminosity of each quasar versus the radio luminosity at 5 GHz of its compact core and find good correlations. This suggests that *compact core radio emission and the UV bump have a common energy source in all quasars*. Using the disk luminosity one has an absolute reference scale to compare objects according to their accretion power. In our UV-radio diagram the quasars split into 4 groups separated by their radio core brightness relatively to the disk luminosity: core dominated quasars (CDQ), lobe dominated quasars (LDQ), radio-intermediate quasars (RIQ) and radio weak quasars.

- For a given disk luminosity the cores of radio loud quasars are brighter than those of radio weak quasars, hence the difference between radio loud and radio weak quasars is established already in the inner parsecs.
- For a given disk luminosity CDQ have the brightest cores due to relativistic boosting.
- AGN must have a disk luminosity $\geq 10^{46}$ erg/sec to be able to become a radio loud quasar and produce a FR II type jet.
- The radio core emission of radio weak quasars scales with the central disk luminosity as well.
- A subsample of flat spectrum variable point sources (RIQ) is substantially fainter than CDQ but almost as bright as the cores of LDQ in a disk luminosity regime $< 10^{46}$ erg/sec, we interpret these sources as boosted radio weak quasars
- The one CSS (3C48) quasar in our sample has a core luminosity comparable to other quasars of the same disk luminosity but a tremendously enhanced total radio flux – the jet is undisturbed in the core but disrupted by environmental effects further out

Together with our previously developed model for the jet core emission, where we added energy and mass conservation of the jet-disk system to the standard emission model, we now can strongly constrain the parameter range for jet models.

- Radio loud cores are the most efficient case of a jet and, given the constraints from the disk luminosity, can only be explained if the energy in magnetic field and relativistic particles represent a large fraction ($\sim 50\%$) of the total jet energy.
- This high power of the relativistic particle distribution in radio loud cores can not be explained by accelerating thermal plasma electrons smoothly into a powerlaw distribution but requires a low-energy cut-off of the relativistic electrons around 50 MeV or the presence of a large population of pairs or both.
- The power of the jet approaches 1/3 of the disk luminosity, therefore the jet is energetically important for the disk structure and evolution.
- The bulk Lorentz factor of the jets are between 3 and 10 and can not be much higher because Doppler boosting would reduce the radio luminosity of the bulk of the poulation too much, and the width of the distribution would be strongly increased by the random orientation of inclination angles.
- For the same reason the dependence of the bulk Lorentz factors on the disk luminosity must not be very strong ($\gamma_\mathrm{j} \propto L_\mathrm{disk}^\xi$ and $|\xi| \ll 0.5$).
- The distribution of cores of radio weak quasars can be explained with the same type of relativistic jets as in radio loud quasars but either the ratio $Q_\mathrm{jet}/L_\mathrm{disk}$ is lower or radio weak quasars simply do not reach the extreme efficiency in accelerating electrons.
- The properties of CDQ and RIQ are consistent with being the boosted counterparts of radio loud and radio weak quasars respectively.

We conclude that the difference between radio loud and radio weak quasars need not necessarily arise from different kinds of jets and disks but may simply be due to the presence of a highly energetic electron population in the jets of radio loud quasars. Given the limits from mass and energy conservation in the accretion flow and assuming that electrons are accelerated from the thermal regime into a powerlaw distribution it is impossible to get more radio emission than what is seen in radio weak quasars. To produce radio loud cores an additional process is required that either shifts the whole relativistic electron distribution towards higher energies or creates lots of additional particles, i.e. pairs. In *Paper I* we suggested that hadronic cascades initiated by high energy proton *pp* or $p\gamma$ collisions might be such a process that could be additionally switched on in radio loud quasars (e.g. due to interactions in the shear layer between jet and ISM). Interestingly, hadronic cascades could explain the high energy gamma-ray emission seen in these objects as well (Mannheim 1993). Secondary pair production was also already successfully applied to model the radio emission of the old nova GK Per (Biermann, Strom, Falcke 1994).

With our estimate of the ratio between jet power and disk luminosity, we are also able to estimate the hidden disk luminosity in FR II radio galaxies. By virtue of this method we can insert FR II sources in our UV-radio correlation and show that LDQ and FR II cores as well as LDQ lobes and FR II lobes coincide in this diagram. This demonstrates consistency of our parameter set and of the FR II/quasar unification scheme. In this context we point out that the lack of FR I quasars in our sample – especially in the low power regime below 10^{46} erg/sec – shows that the difference between FR I and FR II can not simply be due to a decrease in disk or jet power alone. As noted already by MRS there appears to be a critical power of $L_\mathrm{disk} \approx 10^{46}$ erg/sec below which only extremely few – if any – radio loud quasars with FR II morphology exist. This might be an important clue for our understanding of the FR I/FR II dichotomy (see Falcke, Gopal-Krishna, Biermann 1994).

Acknowledgements. HF is supported by the DFG (Bi 191/9). We thank M. Rieke and G. Rieke for valuable suggestions and comments. Continuous discussions with J. Rachen, B. Nath and M. Niemeyer helped to clarify some subtle points in our arguments. We also profited from numerous discussions on 'unified theory' and radio galaxies with Gopal-Krishna. This research has made use of the NASA/IPAC extragalactic database (NED) which is operated by the Jet Propulsion Laboratory, Caltech, under contract with the National Aeronautics and Space Administration.

References

Akuyer, C.E., Ludke, E., Browne, I. et al. 1994, A&A in press
Aller, H.D., Aller, M.F., Latimer, G.E., Hodge, P.E. 1985, ApJS 59, 513
Antonucci, R., Barvainis, R. 1988, ApJ 332, L13
Barthel, P.D. 1989, ApJ 336, 606
Barvainis, R., Antonucci, R. 1989, ApJS 70, 257
Biermann, P.L., Strom, R., Falcke, H. 1994, A&A, submitted
Becker, R.L., White, R.L., Edwards, A.L. 1991, ApJS 75, 1
Teräsranta, H., Tornikoski, M., Valtaoja, E. et al. 1992, A&AS 94, 121
Blandford, R.D., Königl, A. 1979, ApJ 232, 34
Böhringer, H., Voges, W., Fabian, A.C., Edge, A.C., Neumann, D.M. 1993, MNRAS 264, L25
Boroson, T.A., Green, R.F. 1992, ApJS 80, 109 (BG92)
Celotti, A., Fabian, A. 1993, MNRAS 264, 228
Chini, R., Kreysa, E., Biermann, P.L. 1989a, A&A 219, 87
Chini, R., Biermann, P.L., Kreysa, E., H.-P. Gemünd 1989b, A&A 221, L2
Cunningham, C. 1975, ApJ 202, 788
Ekers, R. 1969, Aust. J. Phys. Astrophys. Suppl. 7,1
Falcke, H. 1994, PhD thesis, RFW Universität Bonn
Falcke, H. 1994b, to appear in "Unsolved Problems of the Milky Way", IAU Symp. 169, L. Blitz (ed.), Cambridge University press, 11 pages [astro-ph/9411065]
Falcke, H., Biermann, P. L. 1994a, in "Mass Transfer Induced Activity in Galaxies", Shlosman, I. (ed.), Cambridge University Press, p. 44 [astro-ph/9308030]
Falcke, H., Biermann, P.L. 1994b, A&A, in press (*Paper I*) [astro-ph/9411096]
Falcke, H., Biermann, P. L. 1994c, in preparation
Falcke, H., Biermann, P. L., Duschl, W. J., Mezger, P. G. 1993a, A&A 270, 102
Falcke, H., Gopal-Krishna, Biermann, P.L. 1994, A&A, in press [astro-ph/9411nnn]
Falcke, H., Mannheim, K., Biermann, P. L. 1993b, A&A 278, L1 (FMB) [astro-ph/9308031]
Ghisellini, G., Padovani, P., Celotti, A., Maraschi, L. 1993, ApJ 407, 65
Gregory, P.C., Condon, J.J. 1991, ApJS 75, 1011
Hughes, D.H., Robson, E.I., Dunlop, J.S., Gear, W.K. 1993, MNRAS 263, 607
Kaastra, J.S., de Korte, P.A.J. 1988, A&A 198, 16
Kapahi, V.K.,1990, in "Parsec Scale Radio Jets", Zensus, J.A. & Pearson, T.J. (eds.), Cambridge University press, p. 304
Königl, A. 1980, Phys. Fluids 23, 1083
Kellermann, K.I., Sramek, R., Schmidt, M., Shaffer, D.B., Green, R. 1989, AJ 98, 1195 (KSSSG)
Krichbaum T.P., Zensus J.A., Witzel A., Mezger P.G., Standke K. et al. 1993, A&A 274, L37
Kühr, H., Nauber, U., Pauliny-Toth, I.I.K., Witzel, A. 1981, A&AS 45, 367
Lacy, M., Rawlings, S., Hill, G.J. 1992, MNRAS 258, 828
Laing, R.A., Riley, J.M., Longair, M.S. 1983, MNRAS 204, 151
Lind, K.R., Blandford, R.D. 1985, ApJ 295, 358
Machalski, J. & Magdziarz, P. 1993, A&A 267, 363
Malkan, M.A., Sargent, L.W. 1982, ApJ 254, 22
Malkan, M.A. 1983, ApJ 268, 582
Mannheim, K. 1993, A&A 269, 6
Melia, F., Königl, A. 1989, ApJ 340, 162
McLeod, K.K., Rieke, G.H. 1994, ApJ 420, 58
Miller, P., Rawlings, S., Saunders, R. 1993a, MNRAS 263, 425 (MRS)
Miller, P., Rawlings, S., Saunders, R., Eales, S. 1993b, MNRAS 254, 93
Neff, S.G., Hutchings, J.B. 1992, AJ 103, 1746
e R., Gower, A.C., Hutchings J.B., Talon S., Duncan D., Ross G. 1993, ApJS 86, 365
Rachen, J.P., Biermann, P.L. 1993, A&A 272, 161 (RB93)
Rachen, J.P., Stanev, T., Biermann, P.L. 1993, A&A 273, 377
Rawlings, S., Saunders, R. 1991, Nat 349, 138 (RS91)
Rawlings, S., Saunders, R., Eales, S.A., Mackay, C.D. 1989, MNRAS 240, 701
Saikia, D.J., Shastri, P., Sinha, R.P., Kapahi, V.K., Swarup, G. 1984, JA&A 5, 429
Sanders, D.B., Phinney, E.S., Neugebauer, G., Soifer, B.T., Matthews, K. 1989, ApJ 347, 29

Schmidt, M., Green, R. 1983, ApJ 269, 352
Strittmatter, P.A., Hill, P., Pauliny-Toth, I.I.K., Steppe, H., Witzel, A. 1980, A&A 88, L12
Sun, W.H., Malkan, M.A. 1989, ApJ 346, 68 (SM89)
Unger, S.W., Lawrence, A., Wilson, A.S., Elvis, M., Wright, A.E. 1993, MNRAS 228, 52
Wampler, E.J., Ponz, D. 1985, ApJ 298, 448
Wilkinson, P.N., Tzioumis, A.K., Benson, J.M. et al. 1991, Nat 352, 313
Wilson, A.S. 1992, in: "Physics of AGN", Springer Verlag, W. Duschl & S.J. Wagner (eds.), p. 307

A Appendix: Notes on individual sources

PG 0007+106 (III Zw 2): A very unusual quasar which attracted a lot of interest in the past (Kaastra & Korte 1988 and refs. therein). The radio flux density varies more than a factor 30 and shows flare like events on a timescale of one year. Variability is found at all other wavelengths as well from infrared to x-rays. Past VLBI experiments found some 80% of the total flux in a compact core and a jet like extension at PA 148° (no maps are presented). Unger et al. found a weak component 30 kpc away from the core with the VLA at 1.5 GHz not seen at 5 GHz. The core flux density has varied from 425 mJy to 40 mJy at 8.4 GHz between June 1991 and Oct. 1992 (Patnaik, A., p.c.). Large and fast changes of the polarization angles at 4.8 GHz and 8 GHz, outbursts on a month timescale and variability < 10 days at 37 GHz (no polarization measurements) have been found (Aller et al. 1985, Teräsranta et al. 1992). These are typical signs for boosted jet emission, however, III Zw 2 seems to fall on the extrapolation of the lobe dominated quasars and not of the CDQ. We consider this source as the archetype of the RIQ.

PG 0044+030: This source has a relatively low total flux and appears diffuse elongated on a recent VLA map at 20 cm while at 6 cm only the core prevails (Price et al. 1993).

PG 0157+001: We regard the core flux given by KSSSG (5.9 mJy) of this compact source as an upper limit for a flat spectrum core. The spectrum by Barvainis & Antonucci (1989) of the VLA peak flux does show a very steep spectral index ($\alpha \sim -1$) and there is no indication of a flat component above 1 mJy. In adition the KSSSG core flux would make 0157+001 also a possible candidate for being a RIQ which we think is not justified in light of the spectral form. On the other hand 0157+001 has a host galaxy which is almost face on (Hughes et al. 1993) and hence if the jet axis is related to the rotation axis of the galaxy there is a high probability for getting enhanced emission due to boosting.

0232-042: A triple radio source at VLBI scales with a strong bent. The core flux is from Saikia et al. (1984).

0237-233: This is a GPS with two components (lobes?) at the VLBI scale. The spectrum continues to be steep up to 31 GHz and we can only estimate an upper limit for a flat component of $f_c \approx 0.1$ which seems to be consistent with the overall picture.

0134+329, 3C 48: is a famous CSS. High resolution maps (Wilkinson et al. 1991) show a compact core and a hotspot plus a huge amount of diffuse emission making this source outstandingly bright in total flux. Due to an unusually low core/lobe ratio of 0.007 the core flux is consistent with other radio loud objects. This strengthens the idea that 3C 48 is powered by an ordinary radio jet where disruption by environmental effects close to the nucleus causes an enhancement of the (lobe) radio emission.

0414-060, 3C 110: This source is unresolved (Ekers 1969) and the mean value of .11 for the lobe to core ratio we assigned to this source may be inappropriate (see 3C48) but the spectrum is steep with a slight flattening at higher frequencies which might indicate the presence of a weak flat component.

0710+457, Mkn 376: We took 1.6 mJy as VLA core flux at 5 GHz from Neff & Hutchings (1992). The source is compact (< 0.8") and if the total flux of 21 mJy is correct than Mkn 376 has relatively bright extended emission.

0955+326, 3C232: Akuyer et al. (1994) show a map of a compact $\sim$ 1"source and quote a flattening of the spectrum to $\alpha = -0.2$ between 1.4 GHz and 408 MHz therefore it might be a compact steep spectrum source (CSS) or even a GHz peaked source (GPS) and the assumed value for the core lobe ratio is very uncertain although the source fits into the general trend. The total emission however is at the upper end of the distribution

PG 1008+133: UV-bump fit and M_b yield disk luminosities which differ by more than a factor 20 so that the average disk luminosity is completely uncertain. We excluded this source from our fit to the $L_{disk} - M_b$ correlation.

PG 1211+143: This source was obviously misidentified in KSSSG and we take the fluxes given by MRS.

PG 1206+459: UV-bump fit and M_b disk estimates differ by a factor 100 (same as PG 1008+133).

PG 1309+335: MRS report a total flux density of 54 mJy concentrated in a single core component. The flux was $\sim 35 - 50\%$ brighter than in previous surveys (Gregory & Condon 1991: 40 mJy, Becker et al. 1991:

35 mJy). The spectrum is flat and it is a point source at the VLA. In our diagram it occupies the region around III Zw 2; we consider it a RIQ as well.

PG 1333+176 has a core/lobe ratio of 1.2 in KSSSG indicating variability and very weak extended emission. Nevertheless this source is at the lower end of the radio loud sources and one might speculate that this is another example of a RIQ quasar. The total emission is at the extreme lower end for radio loud sources.

PG 1351+640: This is a variable point source. The flux dropped by a factor of 6 within 4 years (Barvainis & Antonucci 1989). In Fig. 1 it clearly stands out from the normal population but does not quite reach the RIQ. One is tempted to call this source an intermediate RIQ source. The fact that the light curve showed a steady decline over 4 years and not a wiggling around an average value makes it difficult to classify the source at present beacuse our averaging procedure gives a strongly biased result. Using the data of KSSSG only would lower the radio flux substantially although it would still be well above the radio weak population. Like 1333+176 one will need more data to come to an unambigious conclusion. Interestingly McLeod & Rieke (1994) find that this is one out of three sources where the luminosity profile is better fitted by an elliptical than by a disk galaxy.

PG 1407+265: was classified as radio loud by Sanders et al. (1989) which is in clear contradiction to its position in Fig. 1 and we labeled it radio weak especially as the core/lobe ratio (~ 0.4) is fairly high.

1501+106: This source had originally a fitted disk luminosity which was a factor 10 higher than what we estimated from the other luminosity indicators because it was the only object where SM89 made an extreme (high $\dot{M}$) fit to try to hit the strong soft x-ray excess. We now redid this and went only for a good fit to the optical/UV data which lowered the disk luminosity estimate substantially.

PG 1634+706: Barvainis & Antonucci (1989) find a slightly inverted spectrum for the VLA peak flux; thus at least here the assumption of a flat spectrum core seems to be justified.

PG 1700+518: A broad absorption line (BAL) quasar like PG 1411+442, was labeled a RIQ by MRS because of its high total flux which is caused by two compact knots separated by 0.9"where the optical nucleus is close to the brighter radio peak. Considering its core flux this source is not outstanding at all and also lacks the other characteristic features of a RIQ as we define it (pointlike appearance and variability). It appears more likely that like in CSS and GPS environmental effects cause the enhancement of the total radio flux by disrupting a weak radio jet.

E1821+643: It is probably a giant elliptical galaxy in the center of a rich cluster with a very luminous AGN. Radio core and jet structure are seen in the center but the total radio flux is very low (Hills et al. 1992). In our diagram it is placed on the upper end of the radio weak distribution supporting the impression that this is a radio weak jet in an environment usually producing radio loud quasars.

2041-109,Mkn 509: VLA data by Barvainis & Antonucci (1989) indicate a flattening of the spectrum beyond 5GHz so that there is indeed a flat component. We took 1.8 mJy as core flux at 5GHz from Neff & Hutchings (1992).

PG 2209+184: VLA total fluxes for this source (z=0.07) at 5 GHz are reported to be between 120 mJy (MRS) and 290 mJy (KSSSG, claimed to be in error by Miller et al.) with a VLA core flux $> 95\%$ of the total flux and a low brightness knot ($S_{4.8\mathrm{GHz}} \simeq 3$mJy/beam). The spectrum is inverted between 5 GHz and 1.4 GHz ($\alpha = -0.24$). Only recently Machalski & Magdziarz (1993) explicitly identified this source as variable with total fluxes at 5GHz between 116 mJy and 326 mJy. Like III Zw 2 we classify it as a RIQ.

This figure "fig1-1.png" is available in "png" format from:

http://arXiv.org/ps/astro-ph/9411100v1

This figure "fig2-1.png" is available in "png" format from:

http://arXiv.org/ps/astro-ph/9411100v1

This figure "fig3-1.png" is available in "png" format from:

http://arXiv.org/ps/astro-ph/9411100v1

(Fig. 1)

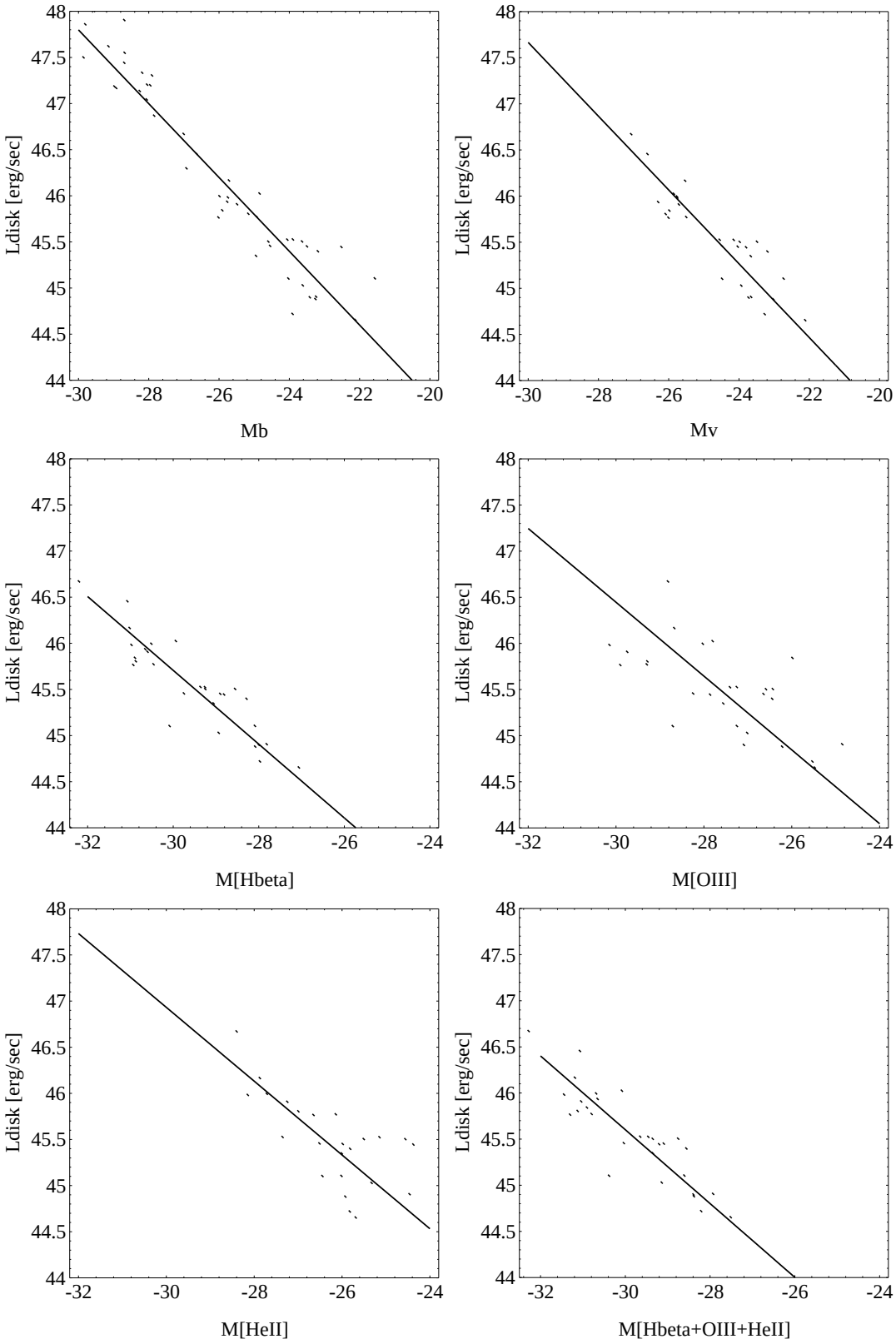

This figure "fig1-2.png" is available in "png" format from:

http://arXiv.org/ps/astro-ph/9411100v1

This figure "fig2-2.png" is available in "png" format from:

http://arXiv.org/ps/astro-ph/9411100v1

This figure "fig3-2.png" is available in "png" format from:

http://arXiv.org/ps/astro-ph/9411100v1

(Fig. 2a)

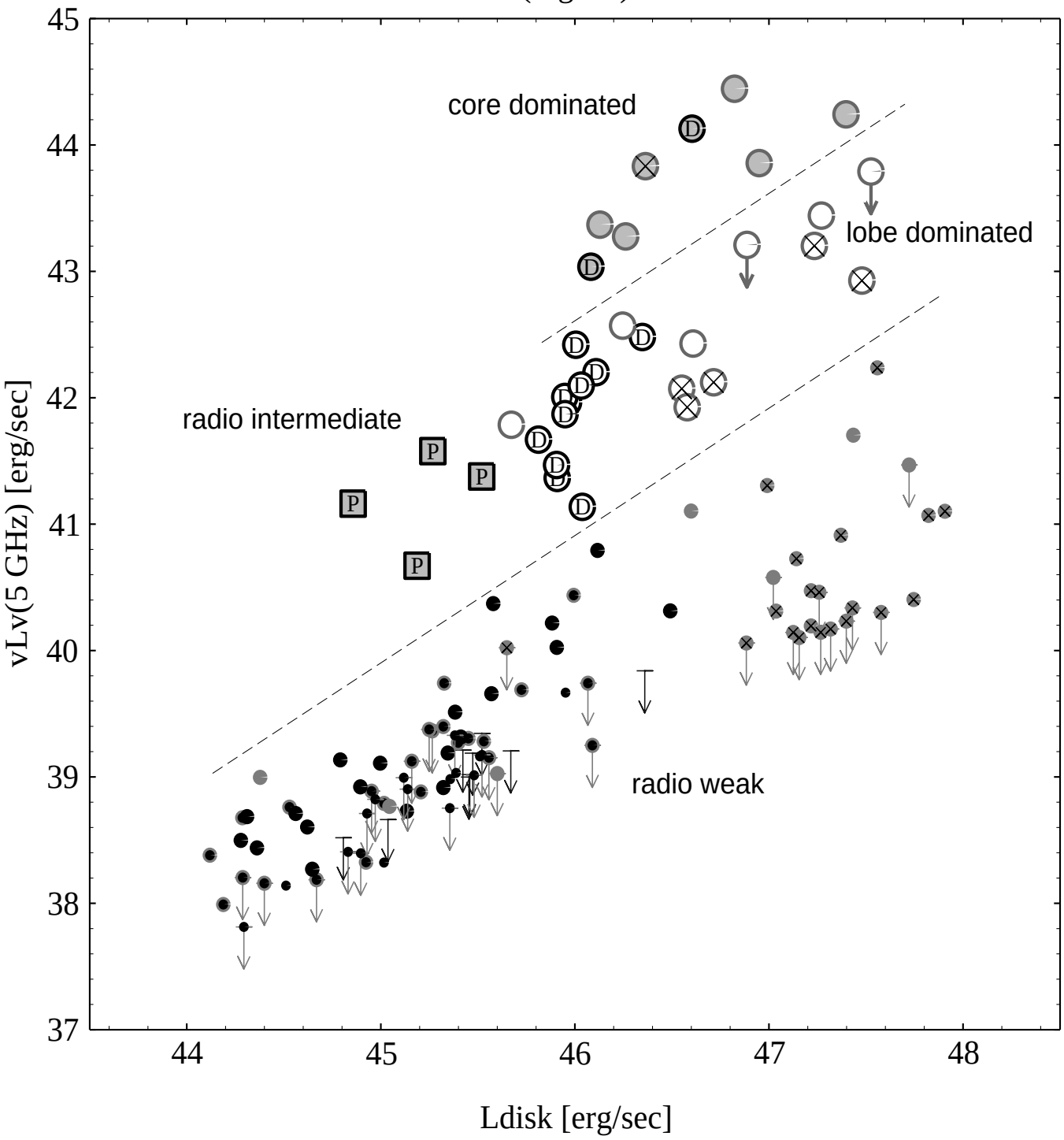
core dominated
lobe dominated
radio intermediate
radio weak
vLv(5 GHz) [erg/sec]
Ldisk [erg/sec]
45
44
43
42
41
40
39
38
37
44
45
46
47
48
D
P

This figure "fig2-3.png" is available in "png" format from:

http://arXiv.org/ps/astro-ph/9411100v1

(Fig. 3a)

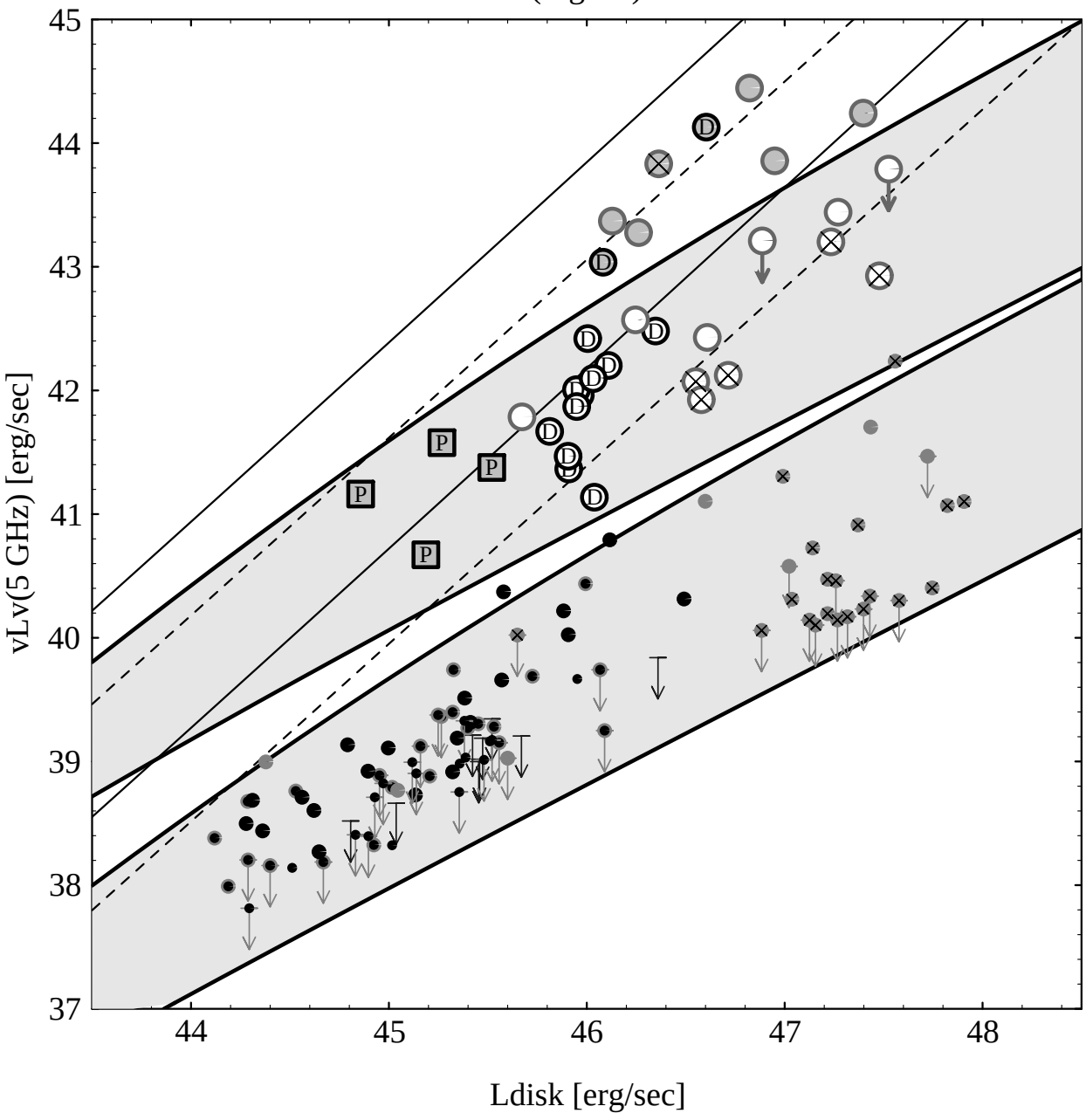
45
44
43
42
41
40
39
38
37
vLv(5 GHz) [erg/sec]
44
45
46
47
48
Ldisk [erg/sec]
D
P

(Fig. 3b)

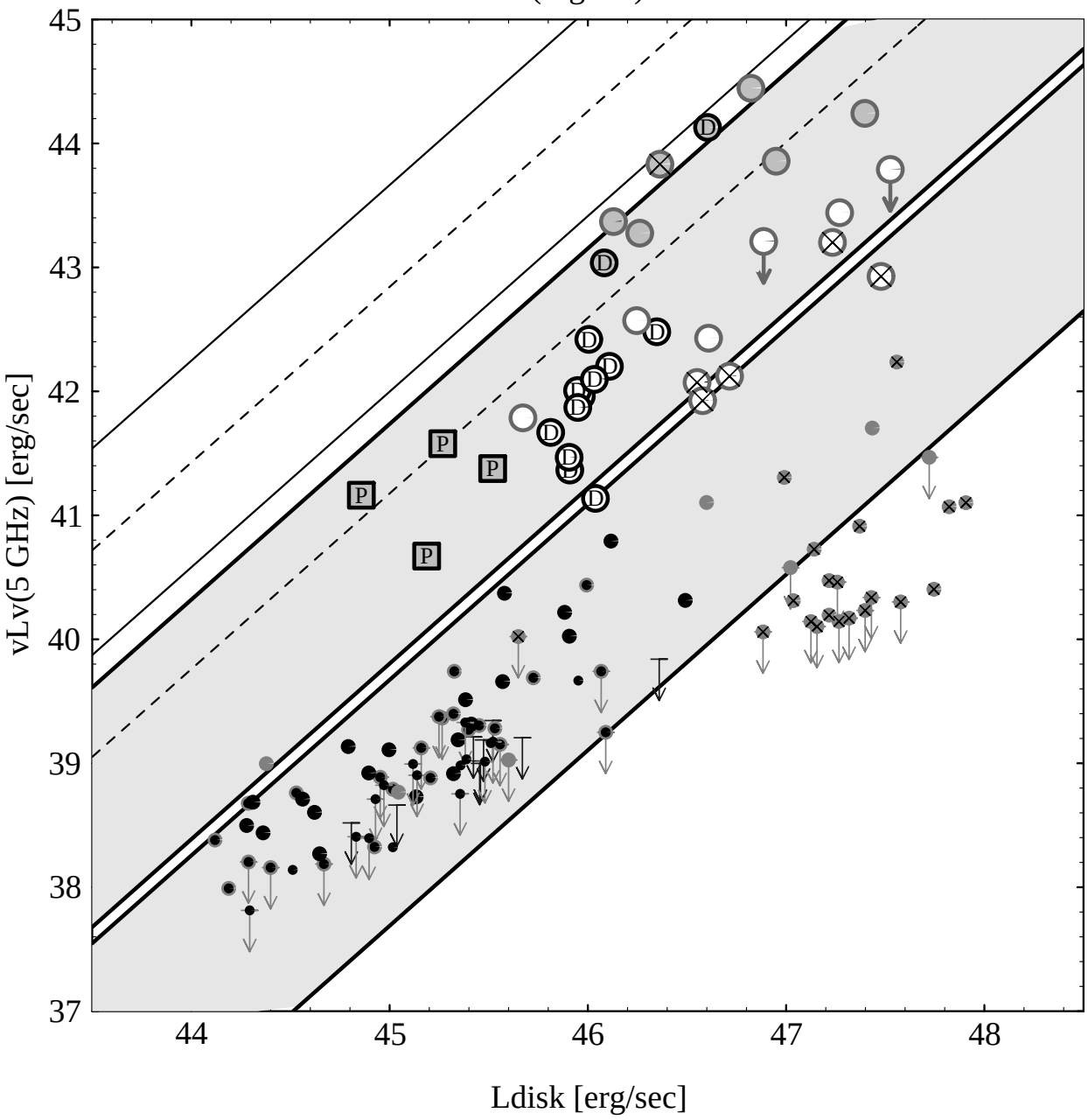
45
44
43
42
41
40
39
38
37
vLv(5 GHz) [erg/sec]
44
45
46
47
48
Ldisk [erg/sec]
D
P

(Fig. 3c)

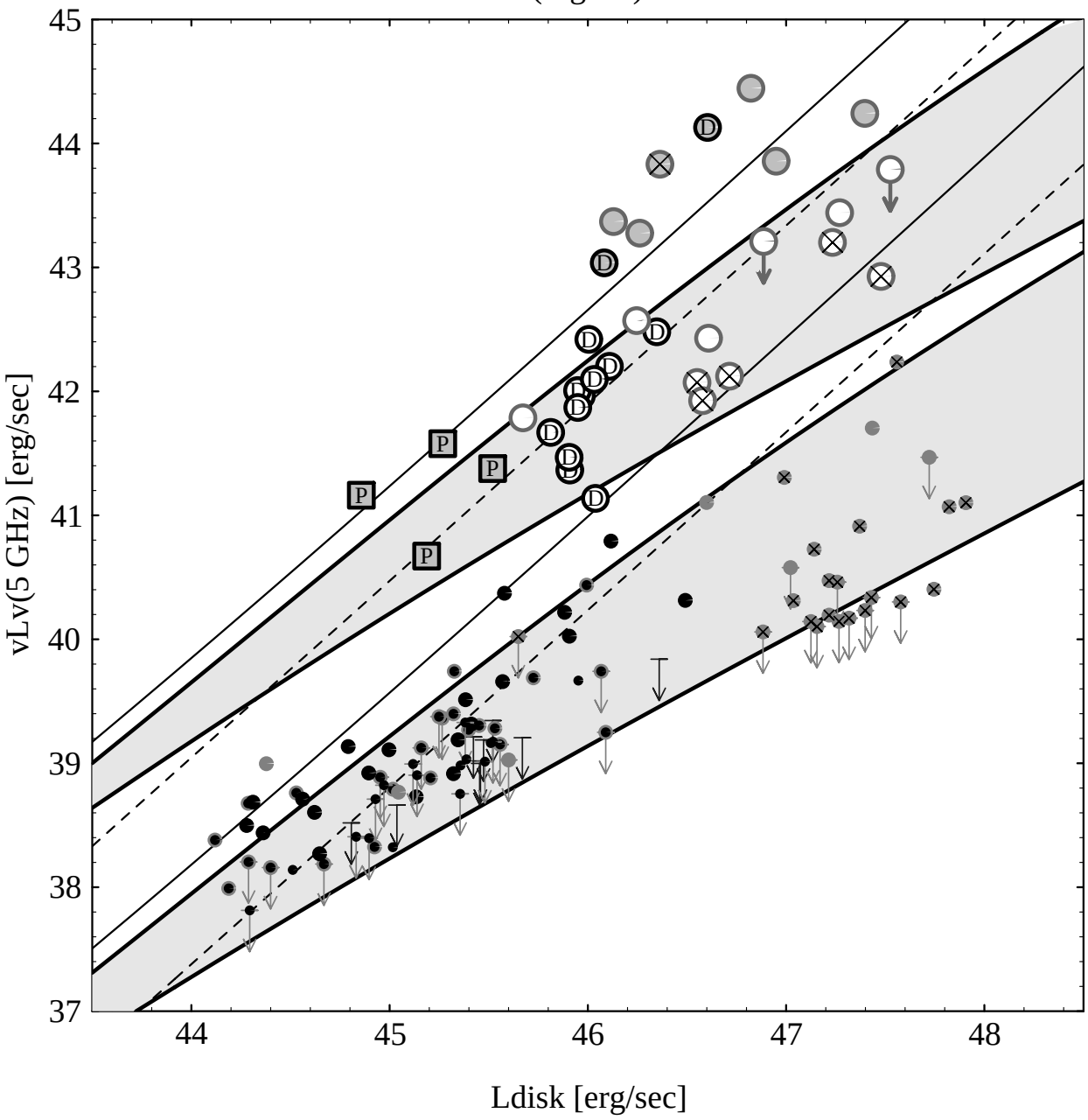
45
44
43
42
41
40
39
38
37
vLv(5 GHz) [erg/sec]
44
45
46
47
48
Ldisk [erg/sec]
P
D

(Fig. 3d)

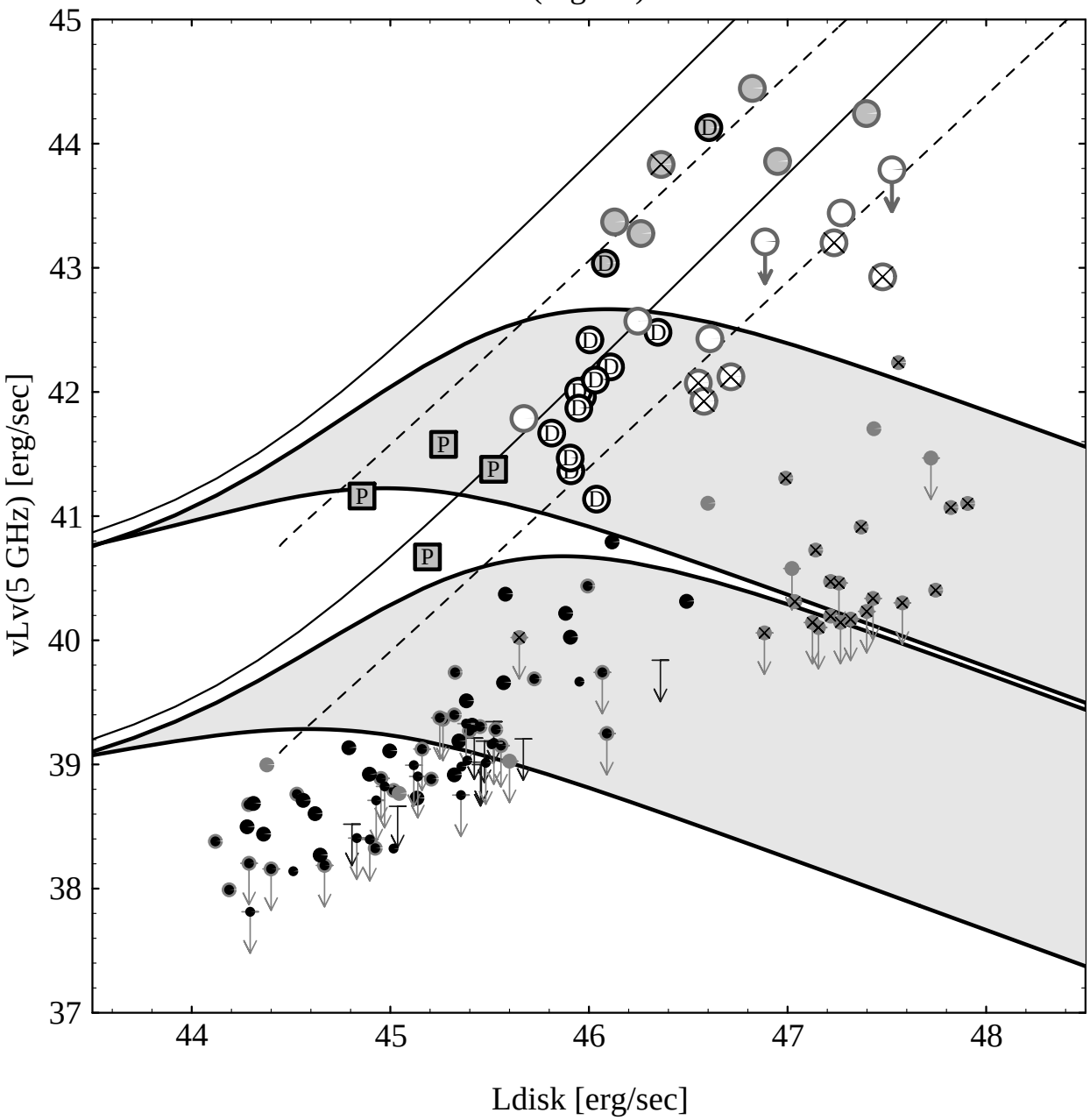
45
44
43
42
41
40
39
38
37
vLv(5 GHz) [erg/sec]
44
45
46
47
48
Ldisk [erg/sec]
D
P

This figure "fig2-4.png" is available in "png" format from:

http://arXiv.org/ps/astro-ph/9411100v1

(Fig. 4)

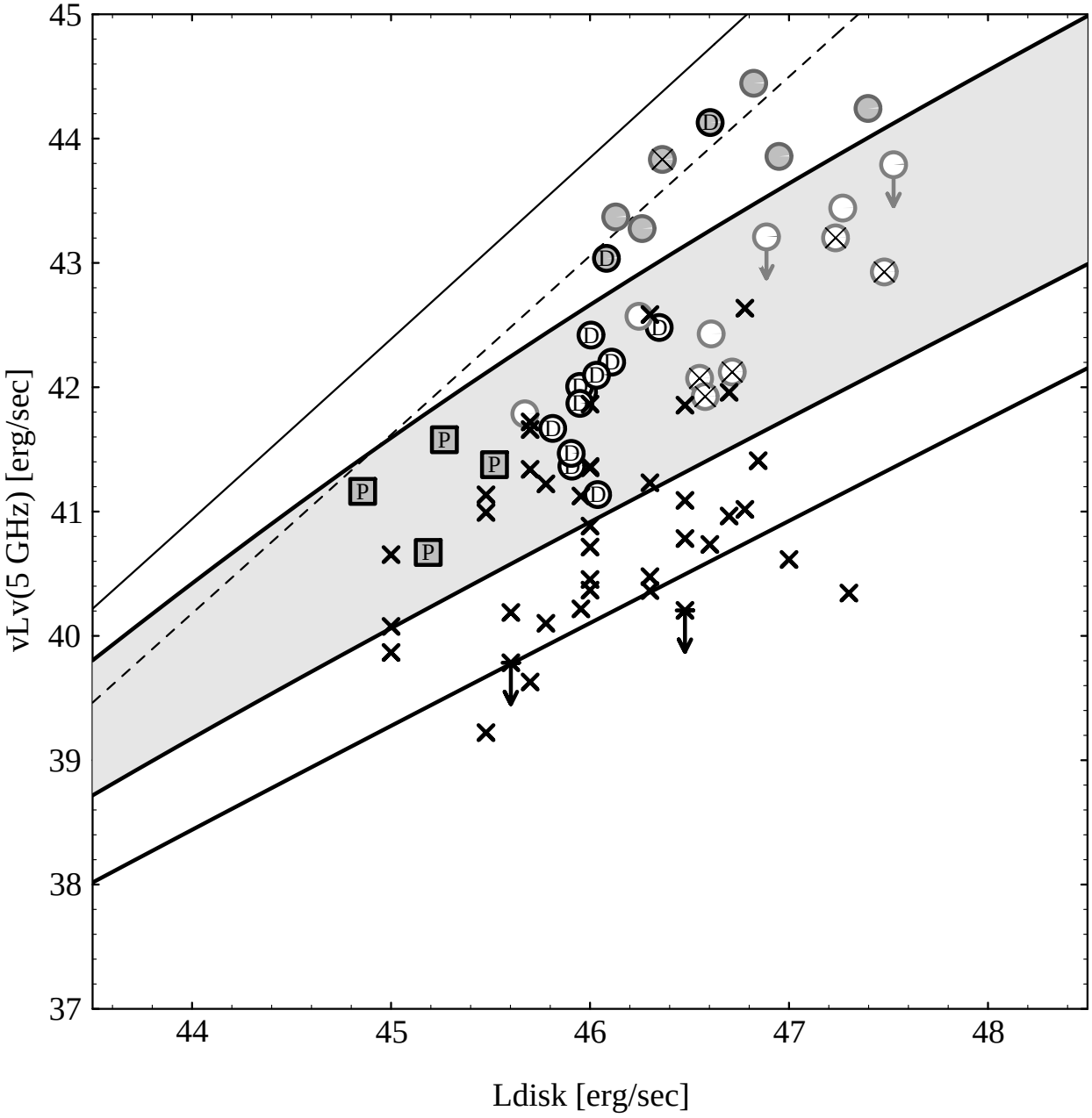
45
44
43
42
41
40
39
38
37
vLν(5 GHz) [erg/sec]
44
45
46
47
48
Ldisk [erg/sec]
D
P

(Fig. 5)